

Coprocessing of 4-(1-naphthylmethyl)biphenyl with Waste Tires Using Finely Dispersed Iron and Molybdenum Catalysts

Ying Tang and Christine W. Curtis
Chemical Engineering Department
Auburn University, AL 36849

ABSTRACT

Coliquefaction of waste tires with coal is a feasible method for upgrading both materials. To evaluate the effect of waste tires on reactions that occur during liquefaction, waste tire and carbon black, a component of tires, were reacted in the presence of 4-(1-naphthylmethyl)biphenyl (NMBB), a model coal compound known to hydrocrack at liquefaction conditions. Waste tires promoted NMBB hydrocracking compared to no additive although carbon black, introduced at the level present in waste tires increased hydrocracking more. Combining Mo naphthenate with waste tire or carbon black had a higher activity for hydrocracking than the corresponding combinations with Fe naphthenate. Selectivity for NMBB cleavage was also different with the two different catalysts. The addition of S increased the activity of Fe naphthenate with waste tire but decreased that of Mo naphthenate. Increased NMBB hydrocracking of 79.9% was obtained by combining Mo naphthenate and carbon black. Combining Fe naphthenate with carbon black or Mo naphthenate did not increase NMBB hydrocracking compared to the values obtained with the individual materials.

INTRODUCTION

Waste tires are waste disposal problems in the United States where more than 240 million tires are disposed of annually. Since waste tires are composed of either natural or synthetic rubber, aromatic oil and carbon black, waste tires are a potential energy source. Waste tires can be coliquefied with coal to produce more valuable end products. Farcasiu et al.^{1,2} demonstrated that coprocessing of used rubber tires and coal produced liquids that are potential sources of transportation fuels or of aromatic oil to be used in new tires. Zondlo and coworkers³ found that the coliquefaction of bituminous coal and rubber tires resulted in greater conversion than did either material individually. Hydrogenation catalysts used by Orr et al.⁴ affected the THF soluble yields of the coliquefied material.

In order to understand more fully how waste tire and carbon black affect the thermal and catalytic reaction of coal at liquefaction conditions, the model species, 4-(1-naphthylmethyl)biphenyl, was used as a model coal compound. In addition, coal and hydrogenation catalysts were used as additives to evaluate their effect on NMBB. The amount and selectivity of the NMBB hydrocracking were used as measures to determine the effect of the different individual additives and combination of additives.

EXPERIMENTAL

Materials. The model NMBB (99% purity) was obtained from TCI America and used as received. The catalysts tested in this study were iron naphthenate (FeNaph) (6% Fe), iron stearate (FeSTR) (9.0% Fe, 98% purity) from Strem, hydrated iron oxide (FeOOH) (63.3% Fe) from Aldrich, and molybdenum naphthenate (MoNaph) (6.0% Mo) from Shepherd Chemical. Three waste rubber samples, GF30 (30 mesh), GF40 (40 mesh) and GF80 (80 mesh), were supplied by Rouse Rubber Industries, Vicksburg, MS. The coal used in the study was Illinois No. 6 bituminous coal from Amoco and carbon black, Black Pearls 2000, was supplied by Cabot Industries. All of the additives to the NMBB reaction were used as received.

Reaction Procedures. Reactions were performed in stainless steel tubular microreactors of ~20 cm³ at 400°C for 30 min with a H₂ pressure of 1250 psig introduced at ambient. The reactor was agitated horizontally at 450 rpm. The reaction system consisted of 0.25 g of NMBB; when additives were used, waste tire, coal or carbon black was added at an equivalent gram amount of 0.25 g. When the relative amount of the additives was changed, the amount of NMBB was held constant and the added material amount was either 5 times 0.25 g or 0.2 times 0.25 g. Catalyst precursors of MoNaph, FeNaph, FeOOH and FeSTR were added at a level of 900 to 1,100 ppm active metal on a per gram of material basis. When dual catalysts of Fe-based precursors and MoNaph were used, the total level of metal was kept constant at 900 to 1100 ppm with Fe:Mo weight ratios of 1:1. When sulfur was added to the reaction, elemental sulfur was added in a 3:1 stoichiometric ratio of sulfur to metal assuming that either Fe₇S₈ or MoS₂ was formed.

The reaction products obtained from reactions of NMBB and the various additives were analyzed by gas chromatography using a Varian Model 3700 gas chromatograph equipped with a fused silica J&W capillary DB-5 30 m column and flame ionization detection. The only products that were analyzed were those from NMBB. The products obtained from NMBB were primarily hydrocracked products; trace amounts of hydrogenated products were detected. Percent

hydrocracking (%HYC) of NMBB was defined as the moles of hydrocracked liquid products as a percentage of total moles of liquid products produced.

RESULTS AND DISCUSSION

Hydrocracking of 4-(1-naphthylmethyl) bibenzyl. The model hydrocracking compound 4-(1-Naphthylmethyl) bibenzyl (NMBB) was reacted noncatalytically and catalytically with and without sulfur in the presence of added material of waste tires, carbon black, and coal as presented in Table 1. A number of different combinations was used to test the effect of the individual additives and combinations of additives on the hydrocracking activity of NMBB. The products produced from NMBB were determined and defined as the lumped parameter, percent hydrocracking. Where NMBB was hydrocracked at the reaction conditions and in the presence of any additive or catalyst used, the primary products obtained were methylbibenzyl (MBB) and naphthalene (NAP). Secondary products, such as naphthyltolymethane (NTM), bibenzyl (BB), methylnaphthalene (MN) and toluene (TOL), were obtained in small amounts as the extent of hydrocracking increased.

The cleavage of NMBB can occur at five different sites which are shown in Figure 1 and are labeled a through e. The selectivity of the bond cleavage that occurred with the different additives is given in Table 1. The primary cleavage that occurred with all of the additives and catalysts was at bond a. In most systems, the second most prevalent cleavage occurred at bond d, with a small amount of cleavage occurring at b. No cleavage was observed at bonds c or e in any of the reactions performed. The selectivity for hydrocracking NMBB at a given bond is given in Table 1 as SA for bond a, SB for bond b and SD for bond d. These selectivities are defined as cleavage at either bond a, b, or d which is divided by the sum of the bond cleavage a, b and d. Therefore, the parameters chosen to compare the results of the different additives and catalysts on NMBB were % HYC, which described the activity for hydrocracking under the specific reaction conditions, and SA, SB, and SD, which reflected the selectivity of the additive or catalyst for NMBB bond cleavage.

Effect of Waste Rubber, Additives and Catalysts on NMBB Hydrocracking. Table 1 presents the effect of different additives and catalysts on NMBB hydrocracking. Initial reactions employed waste tires in three mesh sizes added to NMBB. With increasing mesh size from 30 to 80 and decreasing particle size, the waste tire's effect on NMBB hydrocracking increased from 11.3 to 15.3%. The decreased particle size may have allowed more contact between the reacting NMBB and the active hydrocracking component in waste tire, carbon black. All subsequent experiments were performed with GF 30 waste tire. When the weight ratio of NMBB to waste tire decreased from 1:0.2 to 1:5, the % HYC of NMBB increased from 9.3 to 13.1%, while the selectivity for bond cleavage at a decreased from 91 to 62% with a corresponding increase at d from 9 to 38%. Although the selectivity changed rather substantially with increased waste tire, the change in the total amount of hydrocracking was small.

Since carbon black composes between 20 to 30% of waste tires, the effect of carbon black on the hydrocracking of NMBB was evaluated. Introducing carbon black at a 1:1 weight ratio yielded 79.1% HYC of NMBB. Adding waste rubber or coal at the same level resulted in much less HYC, 11.3 and 7.0%, respectively. A higher ratio of NMBB to carbon black of 1:0.2 was used to approximate the lower amount of carbon black present in waste tire; the amount of HYC achieved was 17.7% which was higher than that obtained with a 1:1 ratio of NMBB to waste tire containing at a minimum 20% carbon black. Likewise, when the ratio of NMBB to waste tire was 1:5 in which carbon black was present in an equivalent amount as in the reaction with a NMBB to carbon black ratio of 1:1, the % HYC was much less yielding 13.1% compared to 79.1%. The carbon black contained in the GF 30 waste tire was not nearly as active as carbon black introduced directly. The selectivity for cleavage at bond a was greater for carbon black than for carbon black in waste tire at equivalent carbon black loadings.

In the coprocessing of waste tire with coal, hydrogenation catalysts would be used to increase the conversion of both coal and waste tire. Two slurry phase hydrogenation catalysts, FeNaph and MoNaph, were used in conjunction with NMBB individually and with additives of waste tire and carbon black. Reactions were performed with and without sulfur. When MoNaph was combined with waste tire, 38.2% HYC of NMBB occurred which was more than double the amount obtained with FeNaph. The addition of sulfur increased the amount of % HYC with FeNaph but decreased the effectiveness of MoNaph. Combining FeNaph or MoNaph with carbon black resulted in high levels of % HYC: 86.4% for FeNaph and 97.9% for MoNaph. The selectivity for cleavage at bond a was greater for Mo than for Fe even when sulfur or carbon black was added.

Ternary systems of NMBB with waste tire and carbon black were reacted without additional catalysts and with three different iron catalysts or MoNaph. The combination of waste tire and carbon black at a 1:0.2:0.2 ratio yielded 29% HYC of NMBB. Addition of MoNaph to this

ternary system increased the % HYC to 71.3% although the selectivity for cleavage at bond a remained high and constant. Increasing the amount of waste tire in the system to a ratio of 1:1:0.2 of NMBB to waste tire to carbon black increased % HYC to an even higher value of 83.5%. Utilization of three types of Fe catalysts at that same ratio resulted in % HYC of 42.6% for FeSTR, 53.7% for FeNaph and 55.2% for FeOOH. All of these hydrocracking values were lower than that obtained for MoNaph.

Reactions with NMBB and waste tires were also performed with combined catalysts containing one of the iron precursors, FeNaph, FeOOH, or FeSTR with MoNaph and sulfur. All three of the reactions yielded % HYC between 16.5 and 20.3% so that the type of iron present made little difference in the hydrocracking behavior of NMBB. The % HYC of 18.5% achieved by the combined catalyst of MoNaph with FeNaph was only slightly higher than the 17.5% HYC yielded by the reaction with FeNaph alone. The selectivity for all of the combined catalysts was very high, ranging from 94 to 98%. The presence of the combined catalysts were not synergistic for promotion of NMBB hydrocracking.

SUMMARY

The NMBB system provided a model for measuring the activity of waste tire and carbon black for hydrocracking. Since NMBB contains C-C bonds that are similar to those present in some coal molecules NMBB can be used to predict the effect of waste tire and carbon black in a liquefaction system containing coal and waste tire. Carbon black introduced directly at coprocessing conditions was highly active for hydrocracking NMBB. When carbon black was present in waste tires, carbon black's activity was much less, indicating that the processing and contact of the carbon black with other material in the waste tires was detrimental to its activity. The combination of MoNaph with either waste tire or carbon black resulted in higher hydrocracking activity and selectivity for cleavage at bond a than did FeNaph. The combination of iron catalysts with MoNaph did not promote hydrocracking of NMBB.

REFERENCES

1. Farcasiu, M., CHEMTECH, January, 22-24, 1993.
2. Farcasiu, M.; Smith, C. ACS Fuel Chemistry Division Preprints, 37, 1, 472-479, 1992.
3. Zondlo, J.W.; Liu, Z.; Dadyburjor, D.B.; Stiller, A.H., presentation in Consortium for Fossil Fuel Liquefaction Science, 7th Annual Technical Meeting, Georgia, 1993.
4. Orr, E.C.; Tuntawiroon, W.; Anderson, L.L.; Eyring, E.M., presentation in Consortium for Fossil Fuel Liquefaction Science, 7th Annual Technical Meeting, Georgia, 1993.

Figure 1. Cleavage Sites for 4-(1-Naphthylmethyl)bibenzyl.

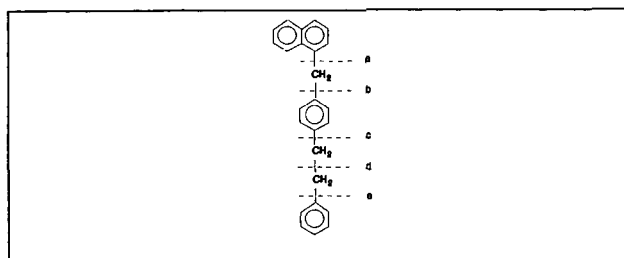


Table 1. Selectivity of the Slurry Catalysts for Hydrocracking 4-(1-Naphthylmethyl)bibenzyl

Reaction Systems	%HYC ^b	Cleavage of a+b+d ^c	Selectivity*100%		
			SA	SB	SD
NMBB (thermal)	4.9±1.3	2.5	61	0	39
NMBB+S	9.3±2.7	4.7	66	2	32
NMBB+GF30WT(1:1)	11.3±2.2	5.7	77	0	23
NMBB+GF40WT(1:1)	13.5±2.5	6.8	76	0	24
NMBB+GF80WT(1:1)	15.3±2.4	7.7	81	0	19
NMBB+WT*(1:0.2)	9.3±2.1	4.7	91	0	9
NMBB+WT(1:5)	13.1±1.7	6.6	62	0	38
NMBB+CB(1:1)	79.1±2.7	39.6	78	6	16
NMBB+CB(1:0.2)	17.7±2.7	8.9	84	4	12
NMBB+Coal(1:1)	7.0±2.1	3.5	83	0	17
NMBB+FeNaph	5.5±1.0	2.8	79	0	21
NMBB+MoNaph	6.4±0.9	3.3	76	0	24
NMBB+FeNaph+S	15.5±1.4	7.7	86	4	10
NMBB+MoNaph+S	39.4±2.3	19.7	92	5	3
NMBB+WT+FeNaph(1:1)	15.5±2.6	7.8	73	0	27
NMBB+WT+MoNaph(1:1)	38.2±2.2	19.2	95	1	4
NMBB+CB+FeNaph(1:1)	86.4±3.8	43.3	89	4	7
NMBB+CB+MoNaph(1:1)	97.9±2.2	49.0	94	4	2
NMBB+WT+FeNaph+S(1:1)	17.5±2.6	8.8	75	0	25
NMBB+WT+MoNaph+S(1:1)	30.1±2.4	15.1	96	0	4
NMBB+CB+FeNaph+S(1:1)	87.3±3.8	43.7	88	6	6
NMBB+CB+MoNaph+S(1:1)	99.7±1.6	49.8	94	5	1
NMBB+WT+MoNaph+S(1:0.2)	29.4±3.0	14.8	98	0	2
NMBB+WT+MoNaph(1:0.2)	13.8±3.0	6.9	97	0	3
NMBB+CB+MoNaph+S(1:0.2)	79.9±3.6	40.0	95	4	1

Table 1. (Continued)

NMBB+WT+MoNaph(1:5)	23.2±2.4	11.7	69	0	31
NMBB+WT+MoNaph+S(1:5)	18.0±2.1	9.1	67	0	33
NMBB+WT+CB(1:0.2:0.2)	29.0±1.7	14.6	92	3	5
NMBB+WT+CB+MoNaph (1:0.2:0.2, 1000 ppm)	71.3±2.5	35.7	95	4	1
NMBB+WT+CB+MoNaph (1:1:0.2, 1000 ppm)	83.5±2.4	41.8	93	5	2
NMBB+WT+CB+FeNaph (1:1:0.2, 1000 ppm)	53.7±2.5	26.9	89	5	6
NMBB+WT+CB+FeOOH (1:1:0.2, 1000 ppm)	55.2±3.0	27.7	95	2	3
NMBB+WT+CB+FeSTR (1:1:0.2, 1000 ppm)	42.6±2.8	21.4	97	0	3
NMBB+WT+FeNaph+MoNaph+S (1:1, 500 ppm each)	18.5±2.1	9.3	98	0	2
NMBB+WT+FeOOH+MoNaph+S (1:1, 500 ppm each)	20.3±2.2	10.2	96	0	4
NMBB+WT+FeSTR+MoNaph+S (1:1, 500 ppm each)	16.5±3.0	8.3	94	0	6

^aWT=waste tire rubber GF30 unless specified; CB=carbon black; MoNaph=Mo Naphthenate; FeNaph=Fe Naphthenate; FeSTR=FeStearate.

^b%HYC is defined as the moles of hydrocracked liquid products as a percentage of the total moles of liquid products produced.

^cCleavage of Bonds a, b, and d is defined as bond cleavage of bond a, b, and d in NMBB.

^dSelectivity is defined as bond cleavage at a (SA) or b (SB) or d (SD) divided by the combined bond cleavage of a, b, and d.

NATURE OF THE CHEMICAL REACTION
FOR FURFURAL MODIFIED ASPHALT

G. Mohammed Memon, FHWA/EBA Engineering Inc.
Brian H. Chollar, FHWA
6300 Georgetown Pike
McLean, VA 22101

Key words: Asphalt/chemically modified, Nature of reaction, Furfural.

INTRODUCTION

Three of the most serious problems of asphalt pavements today are rutting, cracking, and susceptibility to moisture damage (stripping). Asphalt manufacturers have been mixing asphalts with polymers to produce polymer-modified asphalts with improved rheological properties. However, the costs for these improved polymer-modified asphalts are almost double that of regular asphalts. FHWA researchers have found that asphalt modified by the chemical, furfural (which is prepared by simple elimination reaction of aldopentoses obtained from oat hulls), exhibited better stripping properties and was less temperature susceptible than the virgin asphalt,^{1,2} while costing less than polymer-modified asphalts. This paper discusses the possible structure of the furfural-modified asphalt, data for the virgin and furfural-modified asphalts and their Corbett fractions, data from a model reaction between phenol and furfural, and a possible explanation of this structure based on these data.

MATERIALS USED

An Alaskan North Slope asphalt (asphalt A5), obtained from the Strategic Highway Research Program (SHRP), was used. It is an AC-5 asphalt, SHRP number AAV. All of the reagents used were analytical grade from Baxter Scientific Products, McGraw Park, IL, unless otherwise specified.

EXPERIMENTAL METHOD

Furfural Reaction: The furfural-modified asphalt (asphalt A5F) was prepared from asphalt A5 according to the method described by Chollar, et al.² The model phenol-furfural product was prepared by continuously stirring phenol (10 g), furfural (10 g), and concentrated hydrochloric acid (0.19 ml) at 93.3°C for 90 min. The resulting product was analyzed by Thin Layer Chromatography (TLC), Fourier Transform Infrared (FTIR), and High Performance-Gel Permeation Chromatography (HP-GPC).

TEST METHODS

I. ASTM D-4124 (Corbett Analysis): ASTM D-4124 was used to fractionate asphalts A5 and A5F.

II. Thin Layer Chromatography (TLC): The residual furfural starting material in asphalts was detected by TLC using the Benzidine³ and 2,4-Dinitrophenyl hydrazine⁴ spot tests. Visual observation of the resulting colors both with and without ultraviolet (UV) radiation at 254 and 366 nm wavelength was used to detect/differentiate different compounds.

III.a. Reverse-Phase High Performance Liquid Chromatography (RP-HPLC): A Waters HPLC system was used for this study with a 600E brand work station. Methanol or tetrahydrofuran (THF) was used as a solvent at a flow rate of 1 ml/min. A 0.4 ml sample was always injected. Elution of the material was carried out by two methods in an isocratic mode: 1) eluting the sample with methanol for a 10 min period for detecting the furfural starting material, and 2) eluting the sample with methanol from 0 to 15 min, then with THF from 15 to 45 min, and then with methanol from 45 to 61 min to observe the changes which occurred in asphalt A5 and A5F Corbett fractions.

The following procedure was used to determine the starting material (furfural) in Corbett fractions of asphalt A5F by an HPLC technique using reverse-phase chromatography.

1. Asphalt (A5 or A5F, 10mg) was dissolved in 4 ml of 1:1 THF/methanol. The resulting solution was passed through a wet (methanol) Sep-pak C₁₈ cartridge (a reverse phase HPLC technique to rapidly clean the asphalt sample and preserve the life of the RP-HPLC column) and collected. The solution from the Sep-pak was used to obtain the sample for RP-HPLC.
2. THF (2 ml) was passed through the Sep-pak. The solution was

collected in a separate vial. This fraction was used for further investigation.

3. Methanol (2 ml) was passed through the Sep-pak. The solution was collected and used for further investigation.
4. Methanol (2 ml) was again passed through the Sep-pak. The solution was collected in a fourth vial for further investigation.

A calibration curve was made by using different concentrations of furfural in methanol (1, 0.5, 0.25 and 0.125 percent). The solution (0.4 ml) was injected into the HPLC, using method #1 for 10 min in a isocratic mode, eluting in methanol. The peak area for the furfural signal was found at a retention time of 4.85 min and at a wavelength of 252 nm.

III.b. High Performance Gel Permeation Chromatography (HP-GPC): The sample preparation for HP-GPC and the method⁵ used was made according to the method reported by Memon, et al.

EXPERIMENTAL PROCEDURE

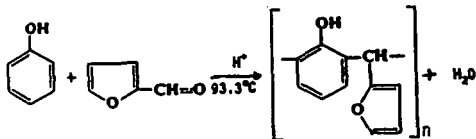
Nuclear Magnetic Resonance (NMR) Spectroscopy: Asphalt samples were dissolved in deuterated chloroform in a concentration of 10 percent (W/V). These were transferred to NMR tubes and were run for ¹H- and ¹³C analysis. A standard coaxial tube containing tetramethylsilane (TMS) was used as a standard.

Three different techniques were used to detect the aromatic/aliphatic carbon and proton ratio and non-protonated carbon atoms present in asphalts A5 and A5F and their polar aromatic and naphthene aromatic fractions: conventional ¹H-, ¹³C distortless enhancement polarization transfer (DEPT), and gated decoupling without nuclear overhauser effect (NOE) ¹³C-NMR.

Fourier Transform Infrared (FTIR) Spectroscopy: The asphalts A5 and A5F were run on a FTIR using neat thin films on a sodium chloride (NaCl) plate. The Stokes analysis⁶ was used to calculate and compare peak areas and ratios to each other in a spectrum. Ratios used for this comparison are shown in figure 10. It has been shown that the 1378-1578 cm⁻¹ region (aliphatic region) does not change significantly for most asphalts including A5 and A5F. Thus, ratios of this aliphatic region to other infrared peak regions for asphalt (A5) will show the increase or decrease in that regional area as compared to the same ratio for asphalt (A5F).

RESULTS

There are several ways in which furfural can react with the phenolic type compounds in asphalt. One of the most probable ways that furfural can react with phenol is by a condensation type of reaction. The model for this is:



We think that this is the type of reaction that is occurring in the furfural-asphalt modification and that this is the type of product that is observed in asphalt A5F. The following data is obtained in support of this product:

1. **Increase of polarity.** Table I gives the Corbett analyses of asphalts A5 and A5F. There is a significant increase in asphaltene (highly polar) and a slight decrease in the polar and naphthene aromatic fractions of the furfural-modified asphalt. Table II gives the results of the TLC analyses of asphalts A5 and A5F. There are changes occurring in the polar and naphthene aromatic fractions using 90 percent methanol - 10 percent toluene. There were no other changes in the other fractions. Therefore, a reaction occurs with a change in the polar and naphthene aromatic fractions of the asphalt. These results show the higher polarity of asphalt A5F.

2. **Furfural consumption.** a. The detection of furfural in the furfural-asphalt reaction was attempted by mixing different amounts of furfural (0.5, 0.38, 0.13, 0.06 and 0.03 ml) in hot asphalt A5 (50 gms) at 57°C on a hot plate for 30 s and observing the separation of the mixtures by RP-HPLC. No signal was observed at 252 nm wavelength (wavelength of the pyrrole ring with the 2-CHO

functional group in furfural) at a retention time of 4.85 min (figure 1, furfural in asphalt at 57°C). Therefore, no free furfural is found in any of the mixtures. b. The detection of furfural was also attempted by mixing different amounts of furfural (0.5, 0.38, 0.13, 0.06 and 0.03 ml) in 50 grams of warm asphalt A5 (26.7°C). The furfural-asphalt mixture (100-150 mg) was analyzed by the above procedure using RP-HPLC. Unreacted furfural was observed in all mixtures at 252 nm wavelength after 4.85 min retention time (figure 1, furfural in asphalt at 26.7°C). c. Asphalt A5 (50 g) was mixed with furfural (0.5 ml) at room temperature. Reverse-phase HPLC was used to analyze this mixture using the above procedure. Figure 1 (furfural in methanol) shows that at 4.85 min, the free furfural signal appeared. The mixture was then heated at 57°C for 30 s and analyzed. There was no furfural signal detected at that time. Thus, the reaction uses furfural and proceeds at temperatures above 27°C. d. The detection of furfural was attempted with asphalts A5 and A5F and their Corbett fractions using the sample preparation method above. These solutions were analyzed by the above reverse-phase method (method #2) and the results are reported in table III. There is no absorption observed at 252 nm in the three fractions of asphalt A5 and A5F at any retention time. These data indicate that furfural has been used in the furfural-asphalt A5 reaction and is not found in any of the Corbett fractions of asphalt A5F.

3. The reaction converts phenolic compounds into substituted phenolic compounds. Rao⁹ has reported that substitution of an -OH group on benzene will give a signal at 270 nm wavelength. A disubstituted benzene shows a signal at 276 nm. O-catechol is an example of this shift, showing a transition at 276 nm. A trisubstituted benzene molecule shows a transition at 287 nm wavelength. The RP-HPLC data for the naphthene aromatic fraction of asphalt A5 shows a small broad signal at 272 nm (table III and figure 2) with 4.7 min retention time in THF followed by methanol (solvent system). This signal may be due to phenol. When the corresponding asphalt A5F fraction was examined, no such signal was detected. This is an indication that a reaction is occurring with phenolic compounds. When the polar aromatic fraction of asphalt A5F was analyzed, a signal at 278 nm was observed in this polar aromatic fraction of asphalt A5F having a retention time of 4.7 minutes in methanol. This signal is possibly the monosubstituted phenolic material (table III).

4. The formation of more polymeric compound of higher molecular size. The GPC data were calculated according to published procedures by P. W. Jennings¹⁰ and reported as percent large molecular size (LMS), medium molecular size (MMS), and small molecular size (SMS), for each asphalt fraction. From the GPC data (table IV), it is clear that there is no significant change in the LMS, MMS, and SMS of asphalt A5F as compared to that of the asphalt A5. Thus, it is not apparent from the analysis if a reaction occurs. Furthermore, table IV demonstrates that the asphaltene fraction of asphalt A5F shows a decrease in LMS and an increase in MMS and SMS as compared to that of the asphaltene fraction of asphalt A5. The data also shows that there is a significant increase in LMS of polar aromatic fraction of asphalt A5F (4%). There is an increase in MMS of naphthene aromatic fraction (0.5%) of asphalt A5F. Thus, significant increases occurred only in the LMS of the polar aromatic fraction of the modified product. Figure 3 shows the changes observed in retention times obtained by RP-HPLC analysis of the naphthene aromatic and polar aromatic fractions of asphalts A5 and A5F. (The TLC analysis confirmed that changes occurred in only the naphthene and polar aromatic fractions). The asphaltene fractions of asphalts A5 and A5F have retention times of 16.5 and 16.8 minutes respectively. This means that there is no significant change in the LMS of the modified asphaltene fraction. The polar aromatic fraction of asphalt A5 begins around 19.5 min, whereas the corresponding asphalt A5F fraction begins around 15.5 min as shown in figure 3. This is an indication that the polar aromatic fraction of asphalt A5F has LMS materials appearing earlier than the corresponding fraction of asphalt A5. The spectrum of the naphthene aromatic fraction of asphalt A5 begins at around 20 min retention time, whereas the spectrum of the same fraction of asphalt A5F begins around 17 min retention time. Again, LMS compounds of the furfural-modified product appear earlier.

The ultraviolet spectra of the SMS of the polar aromatic fractions of asphalts A5 and A5F are in figure 4 and those of the LMS of the polar aromatic fraction of asphalts A5 and A5F are in

figure 5. The spectrum for the asphalt A5 (Figure 4) only shows a signal for phenols at 270 nm. The spectrum for the asphalt A5F fraction only shows a signal at 277 nm (figure 4). This shows the formation of a monomeric monosubstituted phenolic material in the furfural-modified asphalt. Figure 5 shows the presence of tri- or polysubstituted phenolic material of large molecular size (LMS region) in the polar aromatic fraction of asphalt A5F at 288 nm, whereas, there is no such signal in virgin polar aromatic fraction. Thus, it is possible that the furfural-asphalt reaction involves a substitution on the phenol ring in the form of a monomer in the SMS region as well as a polymer in the LMS region appearing in the polar aromatic fraction of asphalt A5F. Substituted phenolic types of compounds showing signals at 277 nm were also observed in SMS of asphaltene as well as naphthene aromatic fractions of furfural-modified asphalt.

The direct reaction between phenol and furfural was conducted under the same conditions as mentioned above. The GPC data shows that this reaction is a polymerization reaction, but it is a mixture of a monomer and a polymer, as is shown in figure 6. The GPC data shows that the model polymer product starts appearing around 22 min retention time, with peaks at 24.1, 28.3 and 30.6 min. A standard pyrene (molecular weight 202, about the weight of the monomer of phenol and furfural), appears around 29 min retention time. The molecular weight of the dimer of the furfural-phenol reaction is 346 and would be expected to be eluted around 27 to 28 min. Thus, the model reaction affords a polymer larger than that of this monomer, a material the same size as the dimer, and a material similar in size to the monomer.

These data showed that there are more large molecular size materials in the polar and naphthene aromatic fractions of asphalt A5F than there are in asphalt A5. These LMS materials in the polar aromatic fraction contain tri- or polysubstituted polymeric phenols. The SMS materials of the naphthene aromatic, polar aromatic, and asphaltene fractions contain monosubstituted monomeric phenols. The model reaction affords a polymer larger than that of the dimer, and a monomer of the size similar to that of the dimer of phenol and furfural. Since the model polymer was prepared under the same conditions as the furfural asphalt reaction, we can assume that furfural is reacting in the same way as the model polymer to give the same type of products.

5. Increase of aromaticity. Using the ^{13}C -NMR gated decoupling technique without NOE, NMR shows a 12 percent increase of aromatic carbon content in the polar aromatic fraction of asphalt A5F versus that of asphalt A5 (figure 7). The proton NMR spectrum of the polar aromatic fraction of asphalt A5F shows a 2 percent higher ratio of aromatic to aliphatic versus that of the polar aromatic fraction of asphalt A5 (figure 9). The infrared data (figure 10) show that the ratio of total aromatic to aliphatic content of asphalt A5F (10/5) is more than that of asphalt A5; the aromatic content of the furfural-reaction product has increased. The infrared data show that the ratio of monomeric to polymeric aromatic content of asphalt A5F (3/1) is less than that of asphalt A5, thus the polymeric substitution of the aromatic ring of the asphalt A5F has increased. These data show that the aromaticity of the asphalt A5F is higher than that of asphalt A5. Therefore, the phenolic groups in asphalt A5 are combining with furfural to produce a higher aromatic material (asphalt A5F) as suggested by the model structure.

6. Increase of non-protonated carbon atoms. Using the effect of the DEPT technique, ^{13}C -NMR showed an increase in the non-protonated carbon atom content of the polar aromatic fraction of the furfural-modified asphalt versus that of asphalt A5 (figure 8). The model structure of the modified product has more non-protonated carbon atom content than that of phenol or phenolic material reactants.

7. Increase of unsaturation. Infrared data (figure 10) show that the ratio of unsaturated to aliphatic content of asphalt A5F (4/5) is higher than that of asphalt A5. As a result, the unsaturated content of asphalt A5F has increased. With the addition of furfural, the model structure of the modified product contains more unsaturated carbon content than that of phenol or phenolic material reactants.

CONCLUSIONS

We have shown that our data for asphalt A5F using the above seven experimental results are consistent with the proposed structure of

the phenol-furfural polymeric product, and that it is possible that the furfural-asphalt reaction for phenolic materials in asphalt A5 is occurring in the same way as is proposed in the model reaction.

FHWA researchers will now pursue other reactions of this type to further improve the properties of asphalts.

REFERENCES

1. D. Kumari, B. H. Chollar, J. G. Boone, and J. A. Zenewitz, Chemical Modification of Asphalt, FHWA Report No. FHWA-RD-91-193, August 1992.
2. B. H. Chollar, G. M. Memon, N. Shashidhar, J. G. Boone, and J. A. Zenewitz, Characteristics of Furfural Modified Asphalt, 73rd TRB Meeting, January 1992.
3. F. Feigl, Quantitative Analysis by Spot Tests, Elsevier, Inc., New York, p.235, 1946.
4. R. L. Shriner, R. C. Fuson, and D. Y. Curtin, The Systematic Identification of Organic Compounds, John Wiley and Sons, Inc., New York, p.235, 1960.
5. G. Memon, J. G. Boone and B. H. Chollar, Furfural Substitutes for Chemical Modification of asphalt, ASTM STP 1241, Philadelphia, 1994.
6. B. H. Chollar, K. T. Tran, D. Kumari, J. G. Boone, and J. A. Zenewitz, Changes occurring in Asphalt in Drum Dryer and Batch (Pug Mill) Mixing Operation, FHWA Publication No. FHWA-RD-88-195, 1989.
7. D. J. Cram and G. S. Hammond, Organic Chemistry, McGraw-Hill Inc., New York, p.385, 1959.
8. C. N. R. Rao, , Calculation of Primary Band Transition($\pi-\pi^*$), J. Sci. Res. (India), vol. 17B, 56, 1958.
9. R. M. Silverstein, G. C. Bassler, and T. C. Morrill, Spectrometric Identification of Organic Compounds, John Wiley and Sons, Inc., New York, p.325, 1980.
10. P. W. Jennings and J. A. S. Pribanic, The Expanded Montana Asphalt Quality Study Using High Pressure Liquid Chromatography, FHWA Report No. FHWA-MT-85-001, 1985.

TABLE I: CORBETT ANALYSIS

Sample name	Asphaltene ± SD %	Polar Aromatics ± SD %	Naphthene Aromatics ± SD %	Saturates ± SD %
Asphalt A5	12.0 ± 1.6	28.3 ± 1.5	41.9 ± 0.1	12.7 ± 1.8
Asphalt A5F	18.3 ± 1.5	27.0 ± 1.9	38.8 ± 0.9	12.2 ± 0.4

Asphalt A5 = Virgin asphalt A5

Asphalt A5F = Furfural modified asphalt A5

TABLE II: THIN LAYER CHROMATOGRAPHIC COMPARISONS OF THE CORBETT FRACTIONS OF ASPHALT A5 AND A5F.

Functions	Asphaltene Fractions	Polar Aromatic Fractions	Naphthene Aromatic Fractions	Saturate Fractions
Observation	same	different	different	same
R _r of A5	same
R _r of A5F	same	0.05 0.55	0.21	

A5 = Virgin asphalt A5 A5F = Furfural modified asphalt A5

R_r = Retardation factor = Not observed

TABLE III: RP-HPLC DATA FOR FURFURAL IN ASPHALT A5 AND ASF AND IN THEIR FRACTIONS

Reten. Time	A5-A-MT	ASF-A-MT	A5-A-M	ASF-A-M	A5-A-TM	ASF-A-TM	A5-A-T	ASF-A-T
4.7MIN	---	225 nm	-- 244 nm	205 nm 235 nm --	-- no signal --		210 nm 215-227 nm 248 nm 262 nm	210 nm --
6.5MIN	202 nm -- 230 nm 260 nm	-- 218 nm -- 260 nm	--no signal --		-- no signal --		200 nm 233 nm 242 nm -- 265 nm	-- -- 245 nm --
	AS-PA-MT	ASF-PA-MT	AS-PA-M	ASF-PA-M	AS-PA-TM	ASF-PA-TM	AS-PA-T	ASF-PA-T
4.7MIN	202 nm	202 nm	210 nm --	-- 278 nm	--	205 nm	--	202 nm
6.5MIN	202 nm	202 nm	-- no signal --		--	203 nm	240 nm	--
	AS-NA-MT	ASF-NA-MT	AS-NA-M	ASF-NA-M	AS-NA-TM	ASF-NA-TM	AS-NA-T	ASF-NA-T
4.7MIN	-- 209 nm -- --	201 nm -- 222 nm 264 nm	209 nm	209 nm	220 nm 240 nm 272 nm	--	-- 220 nm 240 nm 260 nm	212 nm -- --
6.5MIN	203 nm 240 nm	-- --	204 nm 240 nm	-- --	-- no signal --		-- no signal --	

MT = Methanol in tetrahydrofuran TM = Tetrahydrofuran in methanol
M = Methanol T = Tetrahydrofuran
A = Asphaltene fraction PA = Polar aromatic fraction
NA = Naphthene aromatic fraction -- = Not observed

TABLE IV: GPC DATA FOR ASPHALTS A5 AND ASF AND THEIR CORBETT FRACTIONS

Sample	LMS ± SD %	MMS ± SD %	SMS ± SD %
Asphalt A5	20.9 ± 1.2	47.2 ± 0.5	31.9 ± 1.6
Asphalt ASF	20.1 ± 0.8	47.7 ± 0.3	32.2 ± 1.0
A5-AS	42.1 ± 0.5	39.2 ± 0.4	18.7 ± 0.3
ASF-AS	27.8 ± 0.03	44.4 ± 0.08	27.9 ± 0.06
A5-PA	49.3 ± 0.1	36.7 ± 0.4	9.2 ± 0.2
ASF-PA	53.0 ± 0.5	36.8 ± 0.3	10.2 ± 0.2
A5-NA	12.8 ± 0.5	48.5 ± 0.4	38.7 ± 0.04
ASF-NA	12.6 ± 0.03	50.1 ± 0.1	37.3 ± 0.2

LMS = Large molecular size PA = Polar aromatic fraction
MMS = Medium molecular size NA = Naphthene aromatic fraction
SMS = Small molecular size A5 = Virgin asphalt A5
AS = Asphaltene fraction ASF = Furfural-modified asphalt A5

HPLC CHROMATOGRAM

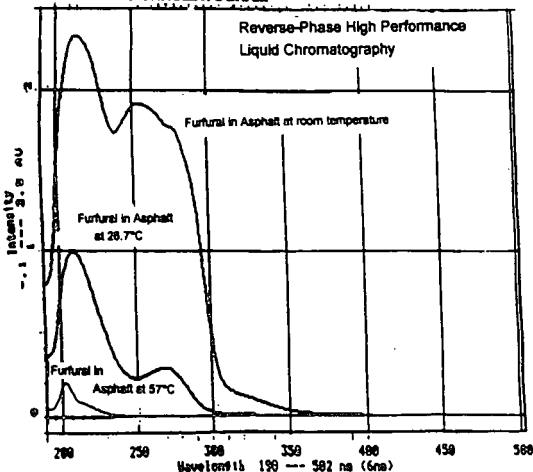


Figure 1: Wavelength spectra of furfural and asphalt for reverse-phase high performance liquid chromatography at a retention time of 4.85 min.

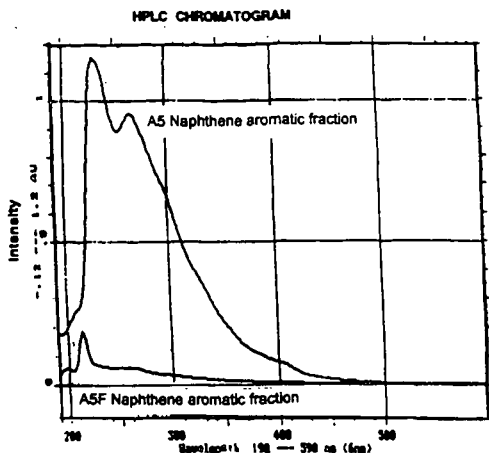


Figure 2: Ultraviolet spectra of the naphthene aromatic fraction of asphalts A5 and A5F from reverse-phase high performance liquid chromatography at a retention time of 4.7 min.

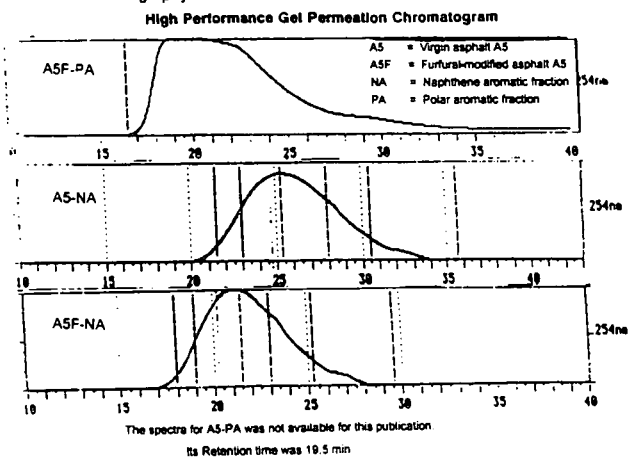


Figure 3: Chromatogram of the naphthene aromatic and polar aromatic fractions of asphalts A5 and A5F.

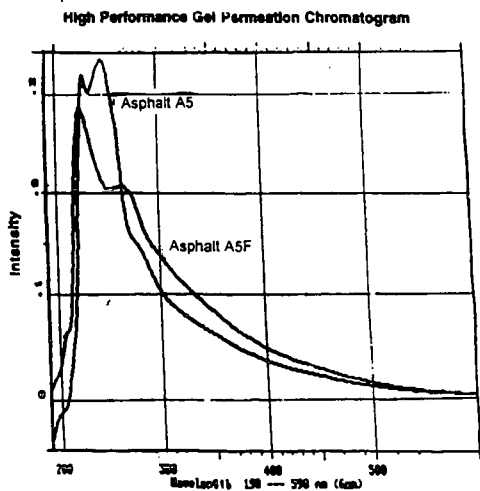


Figure 4: Ultraviolet spectra of the small molecular size polar aromatic fraction of asphalts A5 and A5F.

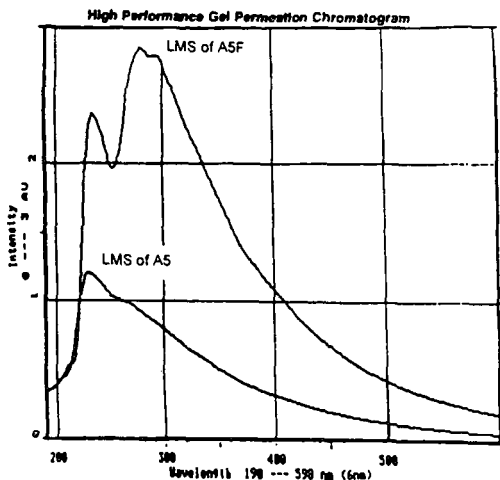


Figure 5: Ultraviolet spectra of the large molecular size polar aromatic fraction of asphalts A5 and A5F.

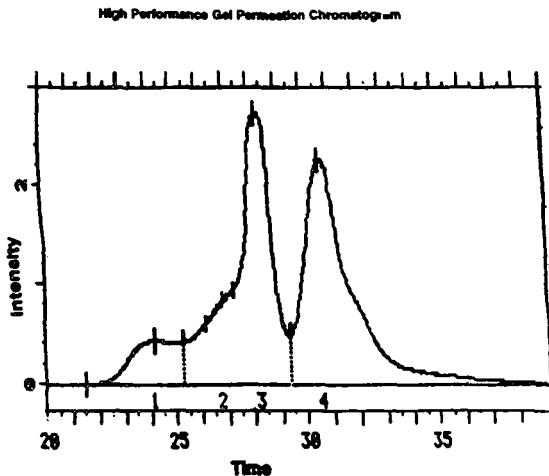


Figure 6: Chromatogram of a model polymer obtained from the reaction between phenol and furfural.

¹³C-Nuclear Magnetic Resonance Analysis

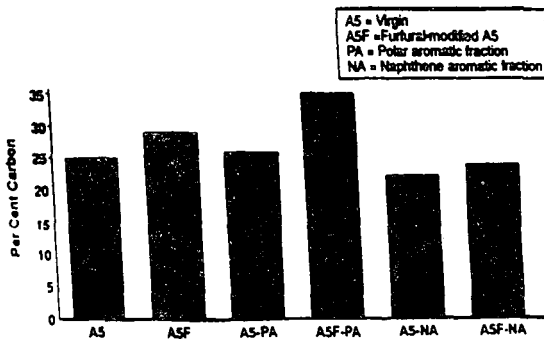


Figure 7: Nuclear Magnetic Resonance data for the percent aromatic carbon content (obtained without the Overhauser effect) present in asphalts A5 and A5F and their Corbett fractions.

¹³C-Nuclear Magnetic Resonance Analysis

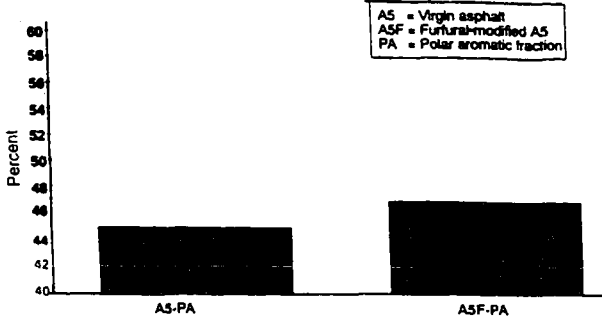


Figure 8: Nuclear Magnetic Resonance data for the percent non-protonated carbon content in polar aromatic fractions of asphalts A5 and ASF.

¹H-Nuclear Magnetic Resonance Analysis

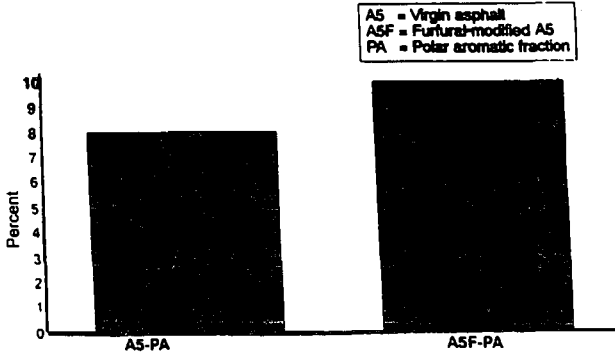
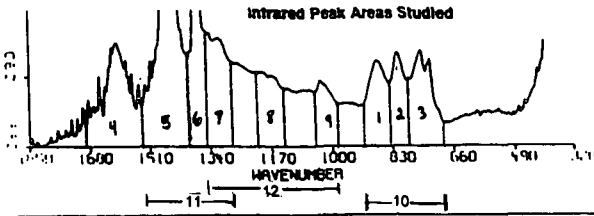


Figure 9: Nuclear Magnetic Resonance data for the aromatic to aliphatic proton ratio of the polar aromatic fractions of asphalts A5 and ASF.



Infrared Peak Area Ratios of Asphalts A5 and ASF

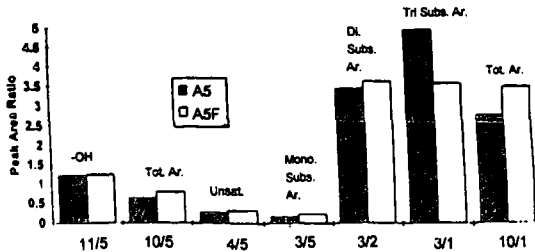


Figure 10: Infrared peak area ratios for asphalts A5 and ASF.

SELECTIVE CATALYTIC SORBENTS FOR NO_x FROM COMBUSTION FLUE GAS FOR PREPRINTS OF THE FUEL CHEMISTRY DIVISION, ACS

A. Rubel, M. Stewart, J. Stencel
University of Kentucky
Center for Applied Energy Research
3572 Iron Works Pike
Lexington, KY 40511-8433

Keywords: coal-based sorbents, selective NO_x capture, combustion flue gas

INTRODUCTION

A process which uses coal-based activated carbons as selective catalytic sorbents for the removal of NO_x from combustion flue gas is under investigation at the University of Kentucky, Center for Applied Energy Research (CAER) (1-3). Flue gas cleanup would be achieved through the selective capture of NO_x at stack temperatures of 70-120°C followed by desorption of a concentrated stream of NO₂ at elevated temperatures (140-150°C). Processing would involve repeated NO_x adsorption/desorption cycles using the same adsorbent carbon.

Numerous investigations have been conducted on the decomposition of NO_x over carbonaceous materials with respect to the heterogeneous reduction of NO_x (4-9). Under the reaction conditions used, the amount of NO adsorbed was less than 2 wt% of the carbon and, due to the high reaction temperatures, 40-50 wt% of the carbon was gasified (2,6). Our work has concentrated on the use of activated carbons as selective sorbents for NO_x at flue gas stack conditions without added chemicals. Our data suggests that an environmentally benign process is possible which eliminates problems associated with ammonia slippage, and provides possibilities for by-product generation such as nitrates for agricultural purposes, nitric acid, or other nitrated compounds.

This paper will discuss NO_x adsorption on coal-based sorbents, catalytic reactions involved in the adsorption process, identification of the desorbed oxide, and the possibility of making HNO₃ from adsorbed NO_x.

EXPERIMENTAL

Instrumentation. NO_x adsorption/desorption profiles were obtained using a Seiko TG/DTA 320 coupled to a VG Micromass quadrupole MS. The two instruments were coupled by a heated (170°C) fused silica capillary transfer line leading from above the sample pan in the TG to an inert metrasil molecular leak which interfaced the capillary with the enclosed ion source of the MS. The TG was connected to a disk station which provided for programmable control of the furnace, continuous weight measurements, sweep gas valve switching, data analysis, and export of data to other computers. The MS has a Nier type enclosed ion source, a triple mass filter, and two detectors (a Faraday cup and a secondary emissions multiplier). The MS was controlled by a dedicated personal computer which was also used to acquire and review scans before export to a spreadsheet for data manipulation.

TG-MS procedures. The TG heating regime used to produce NO_x adsorption/desorption profiles incorporated segments for outgassing, cooling, adsorption, desorption, and temperature-induced desorption. The details of this heating program have been discussed previously (1). Other TG conditions used have also been published (1,2).

The MS was scanned over a 0-100 amu range with a total measurement interval of approximately 30 s per 100 amu; NO (mass 30) or NO₂ (mass 30 and 46) were identified by comparing amu 30/46 ion ratios.

NO_x scrubbing test procedures. NO_x breakthrough profiles were acquired using a 7.2 ml cylindrical reactor loaded with approximately 1 g of sorbent. A small fraction of the effluent gas leaving the reactor was routed to a mass spectrometer for continuous monitoring of gas composition. The sample was outgassed at 300°C for 1 hour with a He purge at a flow rate of 150 ml/min metered at room temperature and pressure. The coal-based carbon was then cooled to an adsorption temperature of 80°C. Once this temperature was achieved, the purge gas was switched to a simulated combustion flue gas containing 2% NO, 5% O₂, and a balance of He. Subsequent to testing, the reactor was cooled and the sorbent retrieved for analysis.

Nitric acid production tests. Activated carbon which had been completely saturated with NO_x was subjected to two different wash solutions, distilled/deionized water and 3% H₂O₂ in distilled/deionized water. The washes were saved for analysis. A control, non-treated sample of sorbent was also washed with both solutions for comparison.

Analytical procedures. The sorbents were subjected to surface area determinations performed on a Quantachrome Autosorb-6 using a N₂ static volumetric flow procedure. Surface areas were calculated using the standard BET equation between relative pressures of 0.05-0.25 (10). Wash solutions from the nitric acid production testing were analyzed by ion chromatography on a Dionex 2020i instrument according to standard procedures. The pH of the wash solutions was determined by ASTM D3838-80.

Materials and simulated flue gas composition. Two coal based activated carbons, produced commercially by steam activation, were tested during this study. For the purposes of this paper, the two carbons will be identified as **a** and **b**. They had N₂ BET surface areas of 460 and 850 m²/g, respectively.

The NO_x adsorption capacity of the activated carbons was determined using the following concentrations of gases during adsorption: 2% NO, 5% O₂, 15% CO₂, 0.4% H₂O and He as the balance. Helium was used by itself during degassing, physisorption, and temperature programmed desorption.

The range of concentrations of flue gases studied during this work are as follows: 0.3 to 2.0% NO or NO₂; 5 to 20% O₂; 0 to 15% CO₂; 0.4 to 6% H₂O and He as the balance. During some tests, the sorbent was pre-saturated with O₂ or CO₂ to determine their contribution to the adsorption mechanism.

RESULTS AND DISCUSSION

Adsorption Capacities and sorbent gasification. Adsorption/desorption profiles, as shown in Figure 1 for sorbent **a** were used to determine adsorption capacities and recycle potential for the two carbons. On exposure to NO and in the presence of O₂ and CO₂, the weight gained in 30 minutes by sorbent **a** was 13.6%. Desorption of NO₂ from the carbon through both physisorption and temperature programmed desorption was confirmed by mass spectra showing a major peak at amu 30 (the primary mass ion for both NO and NO₂) which coincided with the TG monitored weight loss. A peak was also observed at amu 46, a secondary mass ion for NO₂. The temperature at which maximum desorption occurred was 140°C.

Repeated cycling of the sorbent indicated that gasification and adsorption capacity losses were very small. Carbon **a**, subjected to three NO_x adsorption/desorption cycles, lost approximately 1.5% of its total adsorptive capacity (Figure 1). This loss was partially related to a small amount of carbon gasification (0.5-1.0 wt%). Since the temperature at which maximum desorption occurred, 140°C, is significantly lower than the 400°C to which the samples were heated during temperature-induced desorption, these losses can be reduced by lowering the maximum temperature to which the carbons are exposed. Results for carbon **b** were similar to those for carbon **a** except the adsorption capacity for NO_x was slightly less at 10.7 g NO₂ / 100 g carbon.

NO_x scrubbing test. The response of the mass spectrometer (amu 30) during NO_x scrubbing using sorbent **a** showed removal of NO to near the lowest detection limits of the MS over a 16 minute period (Figure 2). This implies that the NO₂ loading on the carbon was 9.1 g NO₂ / 100 g carbon.

Requirements of adsorption. To better understand adsorption mechanisms and requirements, the adsorption capacity of sorbent **a** was determined for various combinations of NO or NO₂ combined with CO₂ and/or O₂, and for NO or NO₂ on carbon pre-saturated with CO₂ or O₂ (Figure 3). The relative capacity for the combination of gases was defined as the amount of adsorption measured for each case with respect to the base case for both NO and NO₂ adsorption. The base case was the adsorption of NO or NO₂ in CO₂ and O₂. The weight gained by the carbon was the same for both base cases.

It was found that O₂ was required for significant NO adsorption and that CO₂ did not interfere with adsorption. Adsorption of NO in CO₂/O₂ was the same as for NO in O₂ alone. Almost no adsorption of NO occurred in the presence of He or CO₂. These data are consistent with other literature which show low levels of NO_x adsorption at temperatures above 200°C and in the absence of O₂ (4-9). Pre-saturating carbon with O₂ followed by NO adsorption in He improved NO adsorption over the comparable He case, but whether this was due to binding of O₂ to the carbon or slightly higher gaseous O₂ levels as a result of the inability to completely purge O₂ from the TG-MS system could not be determined. There was a slight increase in the weight (approximately 0.5 wt%) of the carbon during O₂ pre-treatment. In contrast to NO adsorption, the relative adsorption of NO₂ was found to be nearly independent of the presence or absence of CO₂ and/or O₂. The amount of NO₂ adsorbed in He was only slightly less than

in O₂.

Control experiments for the above series of experiments indicated that O₂, CO₂ and H₂O were not significantly adsorbed on the sorbent (Figure 4). For comparison, results from a base case with carbon exposed to the simulated flue gas containing NO_x, O₂, CO₂, and H₂O is also shown in Figure 4.

Adsorbed Oxide. Since identical weight was gained by the carbon when it was exposed to identical concentrations of either NO or NO₂ in the presence of O₂, the adsorbed oxide must be the same for both cases. During the adsorption of NO in O₂, a significant exotherm was observed which did not occur when NO₂ was used (Figure 5). The heat of adsorption determined from these dta curves was -1.6 kcal/g NO₂ which is consistent with the conversion of NO + O to NO₂. Detection of this heat of adsorption by the instrumentation requires that the reaction occurred at the surface or within the pores of the sorbent, suggesting the carbon's catalytic role in the conversion of NO to NO₂.

Desorbed Oxide. During all our experimentation, MS mass ion ratios were determined by monitoring amu 30/46. This ratio has been determined for all our experimental conditions and for all combination of the gases. As previously stated, mass 30 is the primary ion for both NO and NO₂ while NO₂ also exhibits a secondary mass ion at 46. The 30/46 mass ion ratio during temperature induced desorption, clearly suggests that the desorbed oxide is primarily NO₂ (Figure 6).

Nitric acid production. The catalytic conversion of NO to NO₂ by the carbon and the desorption of NO₂ as the major product suggests that nitric acid production would be a possible by-product of a process using coal-based sorbents for combustion flue gas clean-up. When carbon a, exposed to simulated combustion flue-gas, was washed with either distilled/deionized water or 3% H₂O₂, the pH of the wash solutions decreased dramatically (Table I). This decrease was caused by an increase in the nitrate ion concentrations of the solutions (Table II). More work needs to be done in this area but these results suggest the possibility that nitric acid could be produced directly from the captured NO_x without additional reactions or chemicals.

SUMMARY AND CONCLUSION

NO_x in the presence of O₂ and CO₂ was selectively captured by coal based activated carbons. The measured heat of adsorption indicated that NO present in the flue gas was catalytically converted to NO₂ at the surface of or within the carbon. The desorbed oxide species was identified as NO₂ by mass ion ratios (30/46). The presence of adsorbed NO₂, which can be simply washed from the carbon as nitrate ion, suggests that the production of nitric acid as a by-product is possible. Our research has shown that coal based sorbents have the potential to be used in an environmentally benign process to selectively remove NO_x from combustion flue gas.

REFERENCES

1. Rubel, A.M.; Stencil, J.M.; Ahmed, S.N. *Preprints Symposium on Flue Gas Cleanup Processes*; ACS, Division of Fuel Chem.: Denver, CO, 1993; 38(2), 726-733.
2. Rubel, A.M.; Stencil, J.M.; Ahmed, S.N. *Proceeding of the 1993 AIChE Summer National Meeting*; AIChE: Seattle, WA, 1993; Paper no. 77b.
3. Rubel, A.M.; Stewart, M.L.; and Stencil, J.M. *Preprints Symposium on NO_x reduction*, ACS, Division of Petroleum Chem.: San Diego, CA, 1994; 39(1), 137-140.
4. Smith, R.N., J. Swinehart, and D. Lesnini. *J. Physical Chem.* 63(1959)544.
5. DeGroot, W.F., T.H. Osterheld, G.N. Richards. *Carbon* 29(1991)185.
6. Teng, H., E.M. Suuberg, J.M. Calo, and P.J. Hall. *Proc. 19th Conf. on Carbon*, (1989)574.
7. Suuberg, E.M., H. Teng, and J.M. Calo. *23rd Symposium (International) on Combustion*, The Combustion Institute (1990)1199.
8. Teng, H., E.M. Suuberg, and J.M. Calo. *Preprints of the 200th ACS National Meeting*, Washington, DC, 35,3(1990)592.
9. Gray, P.G., N.J. Desai, and D.D. Do. *Recent Trends in Chem. Rxn Engr.*, B.O. Kkulkarni, R.A. Mashelkar, and M.M. Sharma, eds., Wiley Eastern Ltd., 1(1987)383.
10. Brunauer, S.; Emmett, P.H.; Teller, E. *J.A.M. Chem. Soc.* 1938, 60, 309.

Table I. pH of wash solutions from nitric acid production tests

Wash solution	pH	Wash solution	pH
H ₂ O Control	6.0	3% H ₂ O ₂ /H ₂ O Control	4.8
H ₂ O, Unused C	6.7	3% H ₂ O ₂ , Unused C	6.4
H ₂ O, NO _x exposed C	2.1	3% H ₂ O ₂ , NO _x exposed C	1.9

Table II. Nitrate ion concentration in wash solutions determined by IC

Wash solution	%NO ₃ ⁻	Wash solution	%NO ₃ ⁻
H ₂ O, Unused C	< 1 ppm	3% H ₂ O ₂ , Unused C	< 1 ppm
H ₂ O, NO _x exposed C	0.18	3% H ₂ O ₂ , NO _x exposed C	0.23

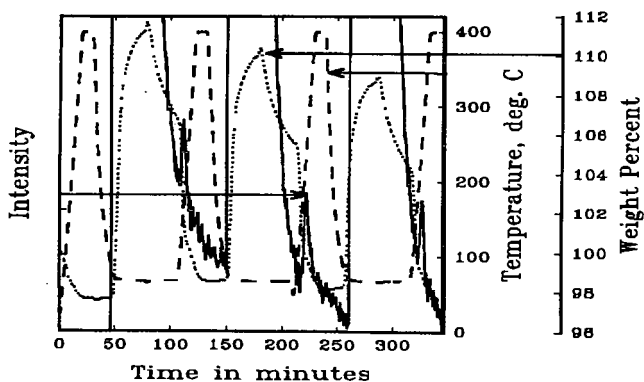


Figure 1. Three cycle ads/des profile for NO_x ads on carbon, a; gases: 2%NO, 5%O₂, 15%CO₂, 0.4%H₂O, balance He

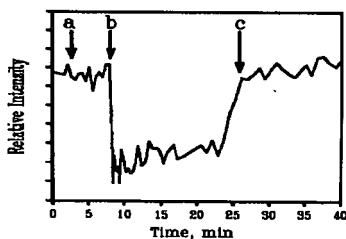


Figure 2. NO_x scrubbing test; mass 30 breakthrough curve; a = baseline NO level, b = gas pass through carbon initiated, c = NO breakthrough

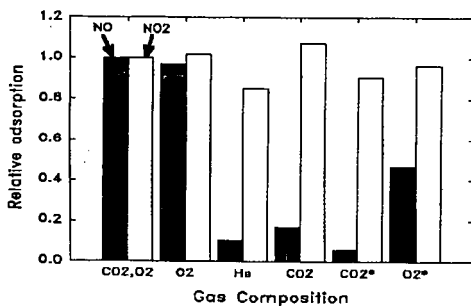


Figure 3. Relative ads of NO_x on carbon, a, in different atmospheres; * = carbon presaturated with O₂ or CO₂; ads in He

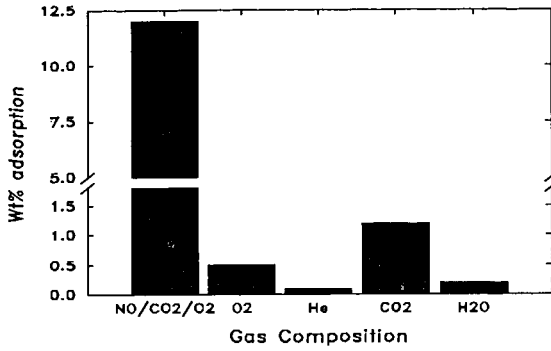


Figure 4. Adsorption of O₂, CO₂, and He on carbon. Gases: 0.6% NO; 5% O₂; 15% CO₂, 6% H₂O; balanced with He

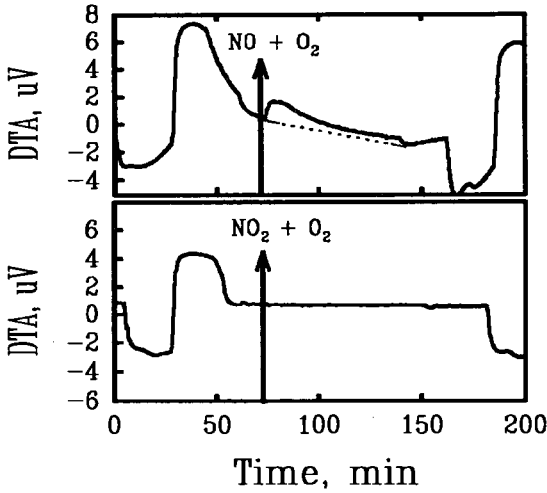


Figure 5. DTA curves for NO vs. NO₂ adsorption in the presence of O₂

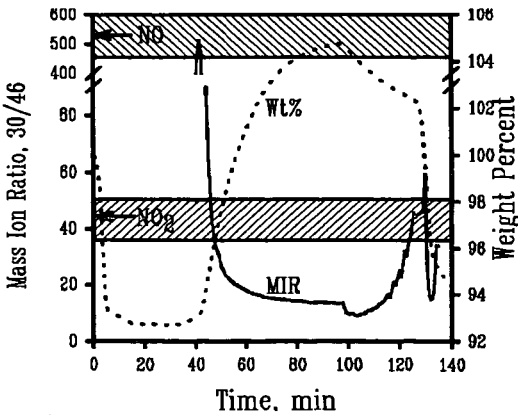


Figure 6. Mass ion ratio (30/46) during desorption

NOVEL APPROACH TO THE PRODUCTION OF GRAPHITE FROM ANTHRACITE

Joseph V. Atria, ShuMing Zeng, Frank Rusinko, Jr., Harold H. Schobert
Fuel Science Program, 209 Academic Projects Building
Pennsylvania State University
University Park, PA 16802

Keywords: Anthracite, Graphite, Optical Microscopy

INTRODUCTION

Currently the carbon/graphite industry uses petroleum coke as the main filler constituent in the manufacture of graphite. Anthracite has been successfully used as fillers for amorphous carbon electrodes, but has not been used in the production of graphite electrodes because of its non-graphitizable structure. Creating a cost-effective graphitizable anthracite, which would have characteristics to be a viable substitute for petroleum coke, would help find an alternative use for Pennsylvania's anthracite and reduce the industry's dependence on petroleum. In the present project, a unique approach to make graphite from anthracite, focused on modifying anthracite's precursor structure by adding a hydrogen-donating substance, has been conducted. This approach is based on two major hypotheses. First, a supply of donatable or transferable hydrogen is needed for the hydrogen-deficient anthracite structure to disrupt crosslink formation between aromatic structures within the coal. Secondly, an aromatic liquid medium is needed to help prevent electronic interactions between aromatic structures and provide the fluidity necessary for aromatic realignment into the graphite structure.

Several hydrogen donors were investigated. 9,10-Dihydroanthracene showed the best ability to donate hydrogen to anthracite and also formed a highly anisotropic anthracene coke in the process. Phenanthrene was selected as the aromatic liquid medium. Both anthracene and phenanthrene have been found to be highly graphitizable [1]. Although hydrogen was successfully donated to the anthracite, the hydrogen donation is believed to have only occurred at the surface and did not affect the internal structure of the coal. Previously treated samples showed good anisotropic character and approached the interlayer spacing of the graphite structure upon heating to graphitization temperatures, but the graphitized anthracites did not show any layering characteristics or crystalline height, L_c [2]. Rouzand and others have found the structure and shape of the initial porosity and flow microstructures of the raw anthracite to be a major factor in the extent of graphitization of anthracite [3]. Because of the dependence of graphitizability on pore structure and the resistance of the internal coal structure to hydrogen donation, six anthracites were studied to determine their pore characteristics. Three of the anthracites, representing a variety of pore characteristics, were then selected to investigate the hydrogenation and subsequent graphitization of the anthracites treated with dihydroanthracene.

EXPERIMENTAL

Six anthracites from various mines in the eastern Appalachian coal region were obtained from the Penn State Coal Sample Bank and Data Base. All of the pore characterization was carried out on 60–100 mesh samples. Helium pycnometry, using a Quantachrome Multipycnometer MVP-1, at room temperature was used to find true densities, weight per unit volume of the pore-free solid. Mercury porosimetry (Quantachrome Autoscan Mercury Porosimeter) was used to obtain the particle density, the weight of a unit volume of solid including pores. Values at 60 psi were taken since interparticle voids are more or less completely filled with mercury at this pressure. The volume percent of open porosity was then calculated from these two density measurements. Macro- and mesopore size distributions were also determined from mercury porosimetry. Both nitrogen and carbon dioxide surface areas were determined, at $-196\text{ }^\circ\text{C}$ and $0\text{ }^\circ\text{C}$ respectively, using a Quantachrome Autosorb-1 automated gas adsorption system. Nitrogen surface areas were calculated using the BET equation. However, the adsorption of N_2 in microporous coals is severely limited and gives appreciably lower values. Carbon dioxide can reach much more of the coals' internal porosity [5]. The Carbon dioxide surface area was calculated using the DR method. Both BET and DR plots showed a greater than 99.5% correlation to a straight line fit. Nitrogen pore volumes were also obtained. Three anthracites were selected for subsequent experimentation: DECS-21, PSOC-1468, and PSOC-1461.

Anthracite samples, -60 mesh, were charged in 20mL capacity stainless steel microautoclave reactors with a mixture of 75% 9,10-dihydroanthracene and 25% phenanthrene, in a 1:2 coal-to-donor ratio. Ratios of higher amounts of dihydroanthracene mixture were also run. Reactions were carried out under 1000 psi nitrogen pressure in a fluidized sand bath. Reactors were continuously agitated to keep the reactants well mixed. A temperature-controlled heat treatment was used: 3h initial hold at $200\text{ }^\circ\text{C}$, temperature increased to $550\text{ }^\circ\text{C}$ at the rate of $5\text{ }^\circ\text{C/h}$, and a final hold at $550\text{ }^\circ\text{C}$ for 2 h. The products were extracted with tetrahydrofuran (THF) for 24h. Optical microscopy samples were then made of the THF-insoluble material and analyzed under a polarized light microscope (Nikon microphot-FXA) with 35mm camera and video ports. Optical micrographs of typical areas were taken. Samples were further heat treated at $1500\text{ }^\circ\text{C}$ for 4h and observed optically then graphitized. Graphitization was conducted at the Carbide/Graphite Group Inc. in St. Marys, PA using an industrial induction furnace. Samples were heated to $2700\text{ }^\circ\text{C}$ and $2900\text{ }^\circ\text{C}$ for 5 hours in purified graphite crucibles. Graphitized anthracite samples were analyzed using optical microscopy again and x-ray diffraction, SCINTAG/USA PAD-V diffractometer with CuK_α radiation. Calculations of the quality and the amount of the sample in the graphite structure were made using X-ray data.

RESULTS and DISCUSSION

The open porosity of the six raw anthracites was calculated from helium and mercury densities and are recorded in Table 1. The mercury densities were calculated using the Washburn equation and all of the densities ranged from 1.53 to 1.63 g/cm³. These values are about 0.2 g/cm³ higher than Mahajan and Walker's results for anthracites. This difference can be explained by the fact Mahajan used de mineralized samples and a smaller particle size fraction, 40-70 mesh [6]. Helium densities ranged from 1.56 to 1.65 g/cm³, except for PSOC-1461 which had a considerably higher density of 1.79 g/cm³. Anthracites have shown the presence of some porosity closed to helium [7]. Curtz and Hirsh also used X-ray studies of anthracites to show interlayer spacings corresponding to true densities of 2.0 g/cm³, as compared to helium densities of 1.5 g/cm³ [8]. PSOC-1461 possibly had a much smaller amount of this porosity closed to helium and therefore gave a much higher density value. Volume percent open porosity values were very small, less than 5.5% with exception of PSOC-1461. PSOC-1468 showed the smallest volume percent of 1.3%.

Surface areas for nitrogen and carbon dioxide are also recorded in Table 1. Considerable care was taken to outgas the coals for over 24 hours due to the difficulties in removing moisture from the microporosity. The microporosity of these anthracite samples is clearly seen by the very low nitrogen surface areas and high carbon dioxide surface areas. Nitrogen surface areas ranged from 0.62 to 4.56 m²/g and were expected to correspond to the amount of open porosity calculations, but PSOC-1467, 1461 and 867 did not show such relationship. Carbon dioxide surface areas were much higher since CO₂ can reach more of the coal's porosity and ranged from 320 and 460 m²/g. DECS-21 showed the largest CO₂ surface area while PSOC-1461 had the smallest surface area.

The very small pore volumes recorded for nitrogen adsorption, Table 2, also point to a very microporous structure. Total pore volumes ranged from 0.9 to 4.6 × 10⁻³ cm³/g. Mercury porosimetry which was taken to 60,000 psi showed only an order of magnitude higher total pore volumes. The mercury intrusion results are also summarized in Table 2. The mercury pore volumes corresponded to the nitrogen volumes except for PSOC-1467. Mercury pore size distributions showed only a very small fraction of macroporosity. Mercury porosimetry can not measure the microporosity. The meso and macroporosity are of interest because this is the porosity which would be intruded by the hydrogen donor. The extensive amount of microporosity and lack of open porosity help point to the difficulties of gaining hydrogen transfer throughout the anthracite structure. There could be many reasons for some of the discrepancies seen in the pore characterization data. Smith and others listed some of the major reasons for the complications in pore characterization, of which the complex pore shapes and connectivities, along with chemical and physical heterogeneities, could easily be reasons for the difficulties in coal characterization [9].

Using the above data, three anthracites were selected for their varying pore characteristics to be further treated with the dihydroanthracene. The proximate and ultimate analyses for these three anthracites is shown in Table 3. DECS-21 was selected for its high CO₂ and N₂ surface area and mid-ranged open porosity. PSOC-1468 was selected for its low open porosity, small N₂ surface area, mid-ranged CO₂ surface area, and low total pore volume with the highest fraction of macroporosity. PSOC-1461 was selected for its high open porosity, and small CO₂ surface area. Table 3 also shows these three samples have very different ash, carbon, hydrogen and oxygen contents.

After samples were reacted, optical micrographs were taken. All three anthracites showed similar optical behavior at this stage; therefore, only the micrographs for DECS-21 (Figure 1) will be discussed. Micrograph (a) shows the anthracite heated to 550 °C without hydrogen donor. The anthracite retains its ridged shape and shows a small amount of inherent anisotropy. Micrographs (b and c) are of the coal reacted with dihydro-anthracene at different magnifications. Micrograph (b) shows how the dihydro-anthracene has been converted to an anisotropic coke which surrounds and binds the anthracite particles together. However, no structural change in the anthracite particles can be seen at this stage. Micrograph (c) shows better the flow domains produced by the mesophase development of the anthracene. This micrograph also shows a very good binding of the anthracene coke to the anthracite. In future work, optical micrographs will be taken of samples heated to 1500 °C and after graphitization to observe if any of the anthracene is imbibed into the anthracite particle and if any structural change of the anthracite has occurred. In addition, X-ray diffraction will be used to classify the quality of the graphite using interlayer spacing and L_c, and to determine the amount of graphitic material present using intensity data.

ACKNOWLEDGMENTS

The authors would like to acknowledge the Carbide/ Graphite Group Inc. for their help in the graphitization of samples and for the financial support for this work provided by the Pennsylvania Energy Development Authority.

REFERENCES

1. T. Sasaski, R. Jenkins, S. Eser, and H. Schobert, *Energy & Fuels* 7, 1039 (1993).
2. J. Atria, S. Zeng, F. Rusinko, Jr., and H. Schobert, Final Report, Pennsylvania Energy Development Authority(PEDA), December 1993.
3. S. Duber, J. Rouzaud, C. Beny, and D. Dumas, Extended Abstracts, 21st Biennial Conference on Carbon, 316 (June 1993).
4. H. Gan, S. Nandi, and P. Walker, Jr., *Fuel* 51, 272 (1972).
5. P. Walker, Jr., and I. Geller, *Nature (London)* 178, 1001 (1956).
6. O. Mahajan, and P. Walker, Jr., Pennsylvania State University, unpublished results (1979).
7. W. Kotlensky and P. Walker, Jr., *Proceedings Carbon Conference* 4th, 423 (1959).
8. L. Cartz, and P. Hirsh, *Philos. Trans. R. Soc. London Ser. A*252, 557 (1960).
9. D. Smith, D. Hua, and W. Earl, *MRS Bulletin* 19, 44 (April 1994).

Table 1. Physical properties of untreated anthracite samples.

Sample	He Density (g/cm ³)	Hg Density (g/cm ³)	Open Porosity volume %	Surface Area (m ² / g)	
				N ₂	CO ₂
DESC-21	1.615	1.530	5.3	4.13	460.4
PSOC-1468	1.653	1.631	1.3	0.92	392.8
PSOC-1467	1.563	1.528	2.2	4.56	379.7
PSOC-1461	1.794	1.549	13.6	2.56	319.7
PSOC-1456	1.562	1.537	1.6	1.31	425.8
PSOC-867	1.635	1.562	4.5	0.62	320.4

Table 2. Nitrogen adsorption pore volume and mercury porosimetry.

Sample	Carbon wt% (daf)	Total Pore Volume x10 ⁻³ (cm ³ /g)	Hg Porosimetry		
			Total Pore Volume x10 ⁻³ (cm ³ /g)	Mesopore Volume x10 ⁻³ (cm ³ /g)	Macropore Volume x10 ⁻³ (cm ³ /g)
DESC-21	90.33	3.7	40.1	39.2	0.9
PSOC-1468	95.36	1.0	28.9	27.7	1.2
PSOC-1467	93.29	4.6	86.0	82.2	2.7
PSOC-1461	93.47	4.2	48.2	48.0	0.2
PSOC-1456	94.56	1.5	31.9	31.6	0.3
PSOC-867	95.07	0.9	27.9	27.9	1.1

Table 3. Analysis of anthracite samples selected.

Sample Seam	DECS-21 Lykens Valley	PSOC-1468 Buck Mountain	PSOC-1461 Mammoth
<u>Proximate Analysis</u> (as rec.)			
% Moisture	3.99	4.51	3.06
% Ash	10.71	6.52	23.44
% Volatile	4.33	3.49	3.89
% Fixed Carbon	80.97	85.48	69.61
<u>Ultimate Analysis (dry)</u>			
% Ash	11.15	6.83	24.14
% Carbon	80.26	88.85	70.87
% Hydrogen	3.56	1.29	1.45
% Nitrogen	0.71	0.78	0.87
% Total Sulfur	0.50	0.49	0.74
% Oxygen (diff)	3.82	1.76	0.89
Atomic H/C (dmmf) PARR	0.5328	0.1744	0.2457
Atomic O/C (dmmf)	0.0295	0.0121	0.0031

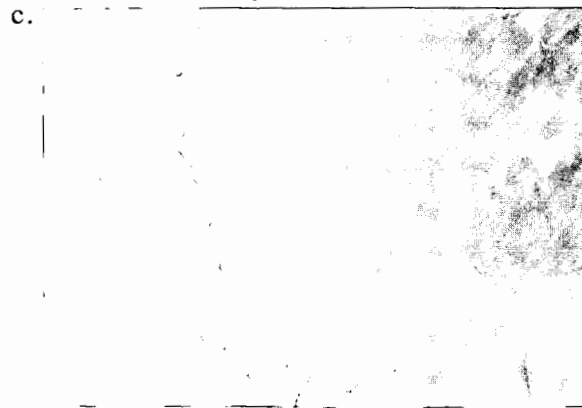
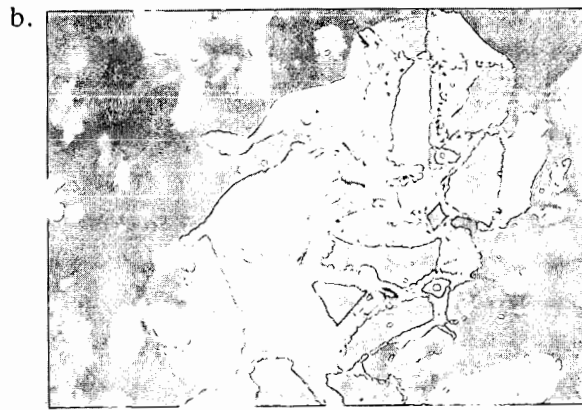
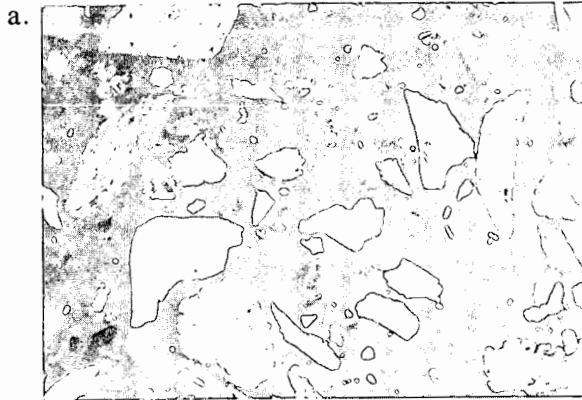


Figure 1. Polarized optical micrographs of anthracite, DESC-21, heated to 550 °C; (a) untreated, 100 X; (b) coal and 9,10-dihydroanthracene, 100X; (c) coal and 9,10-dihydroanthracene, 400X.

KINETICS MODELING OF THE ATMOSPHERIC-PRESSURE CHEMICAL VAPOR DEPOSITION OF SILICON DIOXIDE FROM SILANE AND OXYGEN

Carmen J. Giunta
Department of Chemistry
Le Moyne College
Syracuse, NY 13214-1399

Keywords: kinetics model, oxidation, silane

Abstract

The oxidation of SiH_4 by O_2 is a reaction of interest to chemists in the areas of both combustion and chemical vapor deposition. A detailed kinetics model of this reaction, developed to explain combustion data,¹ is applied with slight modification to kinetic data from atmospheric-pressure thermal chemical vapor deposition (CVD) of SiO_2 films.² The model is also compared to a CH_4 oxidation model under the same CVD conditions, to elucidate differences in the oxidation of SiH_4 and CH_4 under mild conditions. A key difference stems from the rates and major products of the reaction of O_2 with SiH_3 vs. CH_3 radicals.

Introduction

The first serious attempt to model the kinetics of the oxidation of silane by oxygen came from the combustion chemistry community,³ as well as the most comprehensive effort to date (hereafter called BTW after its authors' initials)¹. Meanwhile, materials scientists, electronics engineers, and others have been interested for over 25 years in a controlled version of silane oxidation under mild conditions, an example of the now widely used technique of chemical vapor deposition (CVD).⁴ The interest of this latter group stems from the fact that this reaction can produce thin films of SiO_2 , useful for a variety of purposes in the semiconductor industry and elsewhere.

This paper focuses on a report of the film growth kinetics of such a CVD process, a report rich in kinetic information (deposition rates as a function of distance along the gas flow in the reactor under a variety of concentrations and temperatures) obtained under relatively simple conditions of fluid flow (laminar flow between parallel plates).² The report (hereafter called EH after its authors' initials) is a source of data amenable to modeling, and I attempted to model that data using the BTW mechanism with only slight modification. The conditions employed by EH (atmospheric pressure, low SiH_4/O_2 ratios, mild reaction) are sufficiently different from those for which the BTW mechanism was developed (ignition data over a range of pressures) as to test the robustness of the BTW mechanism.

The questions I addressed are: Can the BTW mechanism adequately model the EH data? How should the mechanism be modified? What are the principal pathways of the mechanism under the conditions employed by EH? How do these pathways differ from those of methane oxidation?

Computational Method

Model growth profiles were obtained by numerically integrating the applicable differential equations for reaction and diffusion in two dimensions. The equations describing reaction in the SiH_4/O_2 system were the mass-action rate equations defined by the 70 reversible elementary reactions among 23 species listed by BTW in their Table I. (I use their numbering in referring to reactions below.) For comparison, the CH_4/O_2 system was represented by 73 reactions total among 19 species. This reaction list is the CH_4/O_2 subset of a mechanism developed to model the CVD of SnO_2 from $(\text{CH}_3)_4\text{Sn}$ and O_2 .⁵ The y dimension is normal to both the flow and the substrate in the horizontal, laminar-flow reactor; the x direction is along the flow, and it represents the temporal evolution of the reaction. Inclusion of the y dimension permitted explicit consideration of the large temperature gradients present in the reactor along that dimension, by allowing for spatially varying rate coefficients. It also facilitated treatment of diffusion normal to the substrate, and direct evaluation of the deposition rate from the diffusive flux onto the growth surface of species which stick to the surface. Details on the computational methods are reported elsewhere.⁶

Results and Discussion

Can the BTW mechanism adequately model the EH data?

The maximum deposition rate in the profiles reported by EH is rather weakly dependent on the temperature of the hot substrate, as shown in Fig. 1; the activation energy is about 27 kJ mol^{-1} over the range 742-845 K. The maximum film growth rate is weakly but inversely dependent on initial oxygen mixing ratio (always in large excess), as illustrated in Fig. 2. And the maximum growth rate is strongly dependent on initial silane mixing ratio, as shown in Fig. 3. If the data (only three data points) define a power-law dependence, the order with respect to silane is around 1.34. Increasing the flow rate pushes the position of the maximum deposition rate downstream and spreads it out, without greatly altering the shape of the profile. Increasing the temperature of the cool wall of the reactor increases the maximum deposition rate only slightly, and does not otherwise alter the shape of the deposition profile.²

The BTW mechanism led to model deposition profiles which reproduce all of the above trends, albeit with higher deposition rates and earlier deposition maxima (discussed below). The activation energy of the maximum deposition rate in the model was about 29 kJ mol^{-1} over the range 742-845 K, as shown in Fig. 1. The peak deposition rate declined slightly but noticeably upon increasing the oxygen mixing ratio from 1.7% to 25%, as illustrated in Fig. 2, although this

inverse relationship seemed to bottom out thereafter. The peak deposition rate followed a power law of order 1.46 with respect to initial silane mixing ratio, as illustrated in Fig. 3. Doubling the flow rate doubled the downstream position of the growth maximum and practically doubled the width of the deposition profile. Increasing the temperature of the cold wall had virtually no effect on the model profile.

Despite the success of the BTW model in capturing the qualitative trends described above, the deposition profiles produced by my model simulations did not greatly resemble the profiles published by EH. (See Fig. 2, which illustrates one of the better resemblances between model and experiment!) In particular, the model profiles peaked too early and too high. To understand this discrepancy, it is necessary to note that in all the model simulations presented here, the temperature was taken to be constant along the x (flow) direction. That is, the short space needed for the gases to warm up to the reactor temperature was neglected. This simplifying assumption facilitated a substantial savings in computational effort and time, and significantly enhanced the numerical tractability of the model's differential equations. However, it also altered the position and magnitude of the maximum deposition rate from what the model would predict if the development of the temperature field had been treated explicitly. The model deposition profiles presented here put the maximum deposition rate very close to the reactor inlet, certainly within the warm-up zone. My experience with modeling another rapid oxidation of silanes^{6b} suggests that treating the transient temperature field explicitly would delay the deposition maximum until the end of the warm-up zone, and spread out the deposition profile somewhat, concomitantly lowering the maximum deposition rate by some 30%. Therefore, the profiles presented here can be expected to have their deposition maxima pushed about 1 cm downstream, spread out, and lowered. These changes would bring the model profiles into much better agreement with the experimental data reported by EH. But a rigorous and quantitative comparison must await simulations in which the development of the temperature field along the flow direction is explicitly treated.

How should the mechanism be modified?

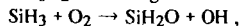
From the viewpoint of reproducing the experimental data, the model profiles should be modified to reduce the deposition peak and move it downstream. That, I expect, will occur with careful treatment of the early temperature field. Still, I considered the BTW mechanism flawed in its treatment of the reaction of the SiH_3 radical with O_2 . The BTW mechanism includes several product channels for this reaction, all proceeding through an excited adduct " $x\text{SiH}_3\text{O}_2$ ", which is included explicitly in the mechanism. First, the rate constant assigned to formation of the adduct (R16 reverse) is two orders of magnitude greater than gas kinetic. Second, the temperature dependence of the effective BTW rate constant for the overall reaction



appears to contradict the only published data on the subject.⁷

The first objection was easily remedied. Running the model with the rate constants for R16 and its reverse reaction decreased by a factor of 100 had no effect on the model deposition profiles. In fact, decreasing the rate constants by a further factor of 50 had a negligible effect. Thus, the BTW model results described above were not limited by the value of the rate constant for formation of the excited adduct $x\text{SiH}_3\text{O}_2$.

The second objection, however, was not so easily resolved. Slagle et al. report a small negative activation energy for reaction (1) over 296-500 K, whereas the effective activation energy in the BTW mechanism is positive over the same range. I tried replacing all the BTW reactions involving excited $x\text{SiH}_3\text{O}_2$ with a single direct reaction

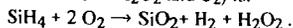


and I assigned to this reaction the rate constant reported by Slagle et al. The resulting model profiles differed negligibly from those discussed above. Thus, not surprisingly, the excited $x\text{SiH}_3\text{O}_2$ (when it was left in the mechanism) functioned as a flow-through species, at least under the modeled conditions. But making $\text{SiH}_2\text{O} + \text{OH}$ the dominant products of reaction (1) is at odds with reports by Koshi et al. that $\text{HSiOOH} + \text{H}$ are the major products (at least at room temperature and 5 Torr).⁸ The BTW mechanism is actually consistent with the product branching ratio reported by Koshi et al., because it assigns a different temperature dependence to the product channels $\text{HSiOOH} + \text{H}$ (R59) and $\text{SiH}_2\text{O} + \text{OH}$ (R60). Thus, the BTW mechanism says that $\text{HSiOOH} + \text{H}$ is the main channel at room temperature but $\text{SiH}_2\text{O} + \text{OH}$ at elevated temperatures; but that temperature dependence conflicts with Slagle et al. The problem is that the model only reproduced the EH data well if $\text{SiH}_2\text{O} + \text{OH}$ was the dominant channel. Yet it did not appear possible to construct rate constant expressions consistent with both Slagle et al. and Koshi et al. that also make $\text{SiH}_2\text{O} + \text{OH}$ the dominant channel at the temperatures employed by EH.

What are the principal pathways of the mechanism?

Model output included concentration profiles for every species. Thus, it was possible to analyze the output to determine which reaction or reactions were primarily responsible for producing and consuming each species. Piecing together these primary pathways allowed me to construct a simplified route from SiH_4 via several intermediates to the deposited film. This scheme for the BTW model under EH conditions is shown in Fig. 4.

The scheme amounts to a branching chain reaction propagated by OH and SiH_3 . SiH_4 was primarily destroyed by OH in a hydrogen abstraction reaction (reaction R13). The resulting SiH_3 radical reacted with O_2 via the flow-through intermediate $x\text{SiH}_3\text{O}_2$ to regenerate OH and produce SiH_2O (R16 reverse). SiH_2O in turn reacted with H_2O produced from reaction R13 above, yielding HSiOOH and H_2 (R62). Successive removal from HSiOOH of the remaining H atoms by reactions with O_2 (R65 and R67) produced SiO_2 , the main film depositing species.* The overall reaction stoichiometry implied by this sequence (assuming that the HO_2 radicals formed in reactions R65 and R67 combine to form H_2O_2 and O_2) is:



But in the model, the HO_2 radicals also provide some branching, for some of them can go back to abstract hydrogen from SiH_4 (R15).

This reduced reaction set (including HO₂ self-reaction, and supplemented by

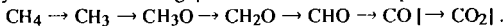
(R23) $\text{SiH}_4 \rightarrow \text{SiH}_2 + \text{H}_2$
to initiate production of reactive intermediates and by

(R11 reverse) $\text{OH} + \text{H}_2 \rightarrow \text{H}_2\text{O} + \text{H}$

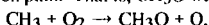
to include all the important reactions controlling OH concentration) was sufficient to capture the main features of the modeled growth profiles presented above. The dependence of the maximum growth rate on both the substrate temperature and the cool wall temperature is small. Its dependence on initial oxygen concentration is small (although, unlike the full model and experiment, positive). And its dependence on initial silane concentration is close to 1.5 order.

How do these pathways differ from those of methane oxidation?

In one sense, comparing principal pathways of methane oxidation and silane oxidation is a bit like comparing apples and oranges, for the two oxidations occur under different conditions. For example, under the concentration and temperature conditions employed by EH, methane oxidation essentially does not occur. To simulate methane depletion comparable to the modeled silane depletion under conditions of identical reactant concentrations, flow velocity, and temperature gradient, a substrate temperature nearly 300 degrees greater was necessary. Under such conditions the main pathway for carbon-containing species was the familiar sequence:

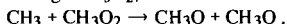


(The final product was a mixture of CO and CO₂). At these temperatures, CH₃ association with O₂ to reversibly form CH₃O₂ was important to the CH₃ budget, but it was essentially a detour from the oxidation path. That is, CH₃O was produced mainly by

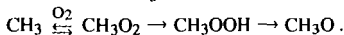


rather than in a pathway leading through CH₃O₂, such as decomposition of CH₃OOH.

Perhaps a more interesting comparison is to examine the oxidation of *methyl* under CVD conditions. Modeling CH₃ oxidation at these lower temperatures showed a different oxidative pathway for CH₃. Here CH₃ rapidly and reversibly associated with O₂, and the path to further oxidation passed through CH₃O₂, via



Of course generating initial CH₃ concentrations equal to the initial SiH₄ concentrations employed by EH under such mild conditions is unrealistic. Still, the importance of CH₃O₂ to methyl oxidation illustrated in this hypothetical case was also seen in the simulations of ref. 5a, in which much smaller CH₃ concentrations arose from decomposition of (CH₃)₄Sn under CVD conditions. In ref. 5a, the sequence that led to CH₃O was:



Both here and in ref. 5a, the relatively low temperature and substantial pressure favored the associative channel in the reaction between CH₃ and O₂ so much that the chain-branching, oxygen-splitting channel to CH₃O was only a minor, even negligible, producer of CH₃O.

In contrast, neither SiH₃O nor a stabilized SiH₃O₂ played an important role in the fate of SiH₃ in the BTW mechanism under EH conditions or in direct studies of reaction (1). Several groups have reported that reaction (1) exhibits no pressure dependence, at least at the low pressures (less than 27 Torr) studied; they interpret this pressure independence as evidence that formation of a stabilized SiH₃O₂ product is negligible.^{7,9} While it is quite conceivable that formation of SiH₃O₂ is negligible at 27 Torr and significant at atmospheric pressure, modeling evidence suggests that this is not the case. I varied the rate constant for SiH₃O₂ formation, and found that when it was a significant channel of the reaction (1), the activation energy of the peak deposition rate was much higher than observed by EH. If SiH₃O₂ played an important role, its decomposition (R36) with a substantial activation energy would contribute to the formation of SiH₂O and subsequent steps on the path to film deposition. Reaction (1) is clearly an important step in silane oxidation, and further study of it is needed, particularly at atmospheric pressure and elevated temperatures.

Conclusion

The BTW mechanism qualitatively reproduced trends observed by EH in the CVD of SiO₂ from SiH₄ and O₂ with respect to temperature, reactant concentration, and flow velocity. A rigorous quantitative comparison of modeled growth profiles to experimental ones must await explicit treatment of the transient temperature field near the reactor inlet. The ability of the BTW mechanism to model CVD data was not lost by changing its rate of SiH₃ association with O₂ to form a flow-through xSiH₃O₂, provided that SiH₂O + OH is the ultimate product of the encounter. The reaction of SiH₃ with O₂ is an important step in silane oxidation, and one which differentiates silane oxidation from methane oxidation. The BTW model was consistent with much but not all the available data on the SiH₃ + O₂ reaction.

References

- ¹Britten, J. A.; Tong, J.; Westbrook, C. K. *Symp. (Int.) Combust., [Proc.]*, 23rd 1990, 195.
- ²Ellis, F. B., Jr.; Houghton, J. *J. Mater. Res.* 1989, 4, 863.
- ³Jachimowski, C. J.; McLain, A. G. NASA Technical Paper 2129: "A chemical kinetic mechanism for the ignition of silane/hydrogen mixtures", 1983.
- ⁴Goldsmith, N.; Kern, W. *RCA Rev.* 1967, 28, 153.
- ^{5a)}Zawadzki, A. G.; Giunta, C. J.; Gordon, R. G. *J. Phys. Chem.* 1992, 96, 5369; ^{b)}Giunta, C. J.; Strickler, D. A.; Gordon, R. G. *J. Phys. Chem.* 1993, 97, 2275. The reactions are listed explicitly under the headings "Hydrogen Oxidation Reactions" and "Hydrocarbon Oxidation Reactions" in Table I of ref. 5b.
- ^{6a)}Giunta, C. J.; Chapple-Sokol, J. D.; Gordon, R. G. *J. Electrochem. Soc.* 1990, 137, 3237; ^{b)}Giunta, C. J. Ph.D. Thesis, Harvard University, 1989.
- ⁷Slagle, I. R.; Bernhardt, J. R.; Gutman, D. *Chem. Phys. Lett.* 1988, 149, 180.

^{8a)}Koshi, M; Miyoshi, A; Matsui, H. *J. Phys. Chem.* **1991**, *95*, 9869; ^{b)}Koshi, M; Nishida, N.; Murakami, Y.; Matsui, H. *J. Phys. Chem.* **1993**, *97*, 4473.

*My implementation of the model allowed SiO₂ as well as every silicon-containing reactive intermediate to deposit if it diffused to the surface. Any partially oxidized silicon intermediates that deposited were assumed to undergo rapid subsequent reaction on the surface to yield SiO₂ film. Unoxidized intermediates like SiH₂ and SiH₃ that deposited were assumed to yield silicon film. Thus, it is not tautologous to state that SiO₂ was the principal depositing species. SiOOH also contributed substantially to the modeled deposit.

^{9a)}Chasovnikov, S. A.; Krasnoperov, L. N. *Khim. Fiz.* **1987**, *6*, 956; ^{b)}Sugawara, K; Nakanaga, T.; Takeo, H.; Matsumura, C. *Chem. Phys. Lett.* **1989**, *157*, 309.

Figures

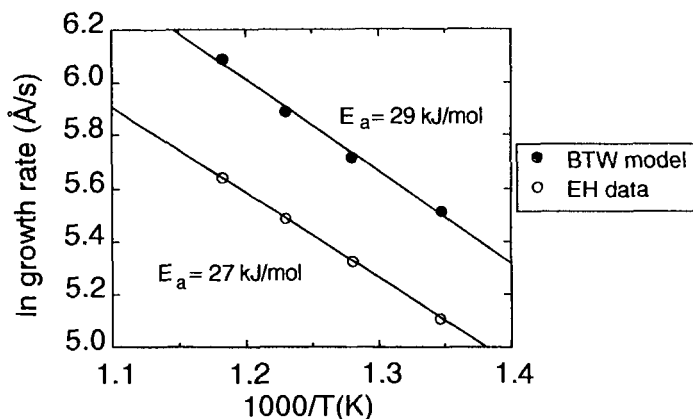


Fig. 1. Arrhenius plot for the peak deposition rate with respect to substrate temperature. Closed circles are model data; open circles experimental data.

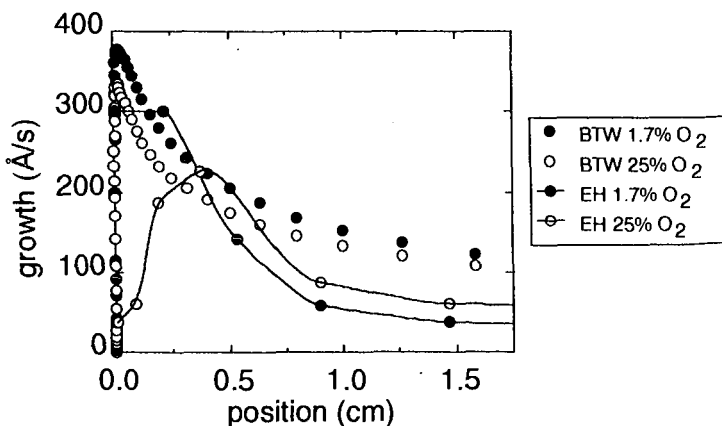


Fig. 2. Model growth profiles under conditions which vary the initial oxygen concentration while keeping the silane concentration constant. Circles without lines are model data; circles with lines are experimental data.

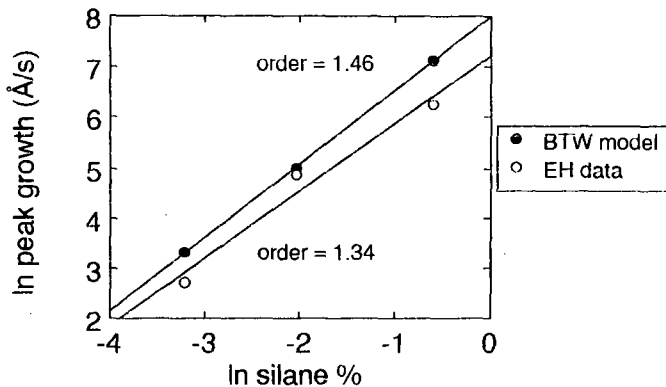


Fig. 3. Plot to determine the order of a possible power law relationship between maximum deposition rate and initial silane mixing ratio. Closed circles are model data; open circles experimental data.

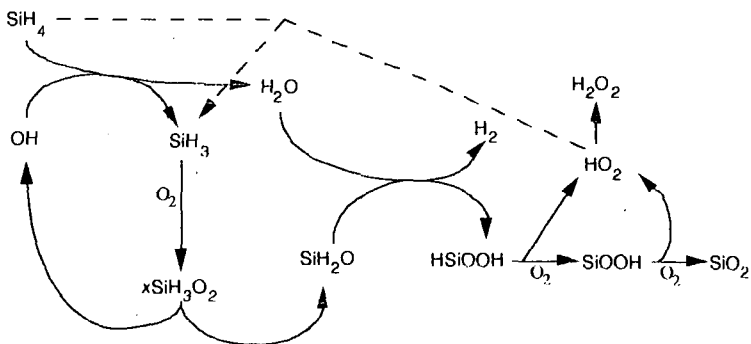


Fig. 4. Major pathways in the BTW mechanism under EH conditions. The solid lines represent primary pathways, and the dashed line branching.

Slagging Behavior of Coal Ash Under Gasifier Environment

Hyung-Taek Kim, Seok-Woo Chung
Department of Energy, Ajou University
5 Wonchen-Dong, Suwon, 441-749, Korea

Shi-Hoon Lee
Korea Institute of Energy Research
P.O.Box 103, Yousung, Daejon, 305-343, Korea

Keywords : Coal Gasification, Slagging, Fusion Temperature

Abstract

For the six different bituminous coals, the fusion temperature and chemical composition of coal ashes are determined. The slagging behavior of each coal ash is estimated by calculating two different slagging parameters. Accurate prediction of slagging behavior with calculated slagging parameters is difficult because of complex ash melting behavior in the high temperature gasifier environment. It will be suggested that the optimum slagging condition for gasifier operation should be determined by measuring strength and deposition rate of slag in the specially-designed DTF(drop tube furnace) which is simulating 3 T/D BSU entrained-bed gasifier condition.

INTRODUCTION

Recently, thermal power plants in Korea are utilized large amounts of imported bituminous coal for their energy source. Because of different characteristics of imported coal, standard ASTM ash composition measurements are used to predict slagging behavior of coal ash in the power plant. However, the estimation of ASTM method doesn't show actual slagging/fouling behavior of coal ash because of complex ash melting behavior in the high temperature [1].

The objective of this study is to predict slagging behavior of coal ash from its physical and chemical properties and to construct a fundamental database by investigating the relationship of chemical composition, fusion characteristics and deposition strength of coal ash. The experimental results are obtained by utilizing ASTM method as well as DTF(drop tube furnace) which simulating an entrained-bed gasifier's temperature and residence time. The results will be used in determining optimum operating condition of slagging gasifier which is the major part of Integrated Gasification Combined Cycle(IGCC). Another objective of the study is intended to prevent clogging phenomena of gasifier slag at gasifier outlet which occurs due to solidification of melted slag. The result of this study can also contribute to the selection of candidate coal in the 3 T/D BSU(Bench Scale Unit) gasifier which is in the construction stage in Korea.

EXPERIMENTAL METHOD

In the systematic investigation, proximate and ultimate analysis of six different coals are conducted and the results are shown in Table 1. All the coal samples are presently used as fuel in Korean thermal power plant. Rank of the coal samples show wide range between sub-bituminous to bituminous.

Analysis of coal ash characteristics, such as chemical composition and fusion temperature, is performed in order to predict slagging behavior of coal ash. Initially, coal ash samples were made using ASTM standard ashing method [2]. Coals are heated from room temperature to 500°C during 1 hour, then to 750°C during 2 hour and leave for no more mass change at 750°C. Chemical composition data of each coal ash is shown in Table 2. The acidic oxide constituents, such as SiO₂, Al₂O₃ and TiO₂ are generally considered to produce high melting temperatures. Whereas, ash melting temperatures will be lowered proportionally with relative amounts of basic oxides of Fe₂O₃, CaO, MgO, Na₂O and K₂O. Coal ash samples are shown wide range of oxides composition as in Table 2. Counting the fact that coal with low fusion temperature of coal ash has a higher propensity of slagging, it can be

predicted that Alaska coal with low contents of acidic oxide consistents and ROTO coal with high contents of Fe_2O_3 will have a higher slagging behavior than others.

The fusion temperature of each coal ash was also measured by using ash fusion determinator (LECO-600). The cones were manufactured to pyramidal shape, height 19mm, base 6.5mm. The experiment was done with reducing and oxidizing conditions, with preheating temperature of 390°C, start temperature of 538°C, final temperature of 1600°C and heating rate of 8 °C /min. The surrounding gases were used of H_2 and CO_2 mixture (50/50) in reducing condition and air is used in oxidizing condition. The result of ash fusion temperature measurement is shown in Table 3. The result of fusion temperature experiments represents same ash fusion behavior as determined by chemical composition data.

RESULTS AND DISCUSSION

Prediction of slagging behavior of coal ash was determined two different methods. Base/acid ratio is to be used as one of the indicators to predict slagging propensity of coal ash, which is defined as follows [3].

$$B/A = \frac{Fe_2O_3 + CaO + MgO + Na_2O + K_2O}{SiO_2 + Al_2O_3 + TiO_2} \dots\dots\dots (1)$$

The calculation of slagging indicators (R_s) using B/A ratio is as follows.

$$R_s = B/A \times \text{Total sulfur} \dots\dots\dots (2)$$

If the R_s value is less than 0.5, the possibility of slagging is low, more than 0.7, the slagging possibility is high and above one, the slagging propensity is severe. The R_s values of the coal ashes used in the experiment are shown in Fig. 1.

The slagging index(F_s) suggested by Gray & Moore is calculated as follows [4].

$$F_s = \frac{4(IDT) + HT}{5} \dots\dots\dots (3)$$

Comparing F_s value with slagging behavior, if F_s value is from 1505°C to 1615°C, slagging possibility is low, from 1325°C to 1505°C, slagging possibility is high and less than 1325°C, the slagging possibility is severe level. The F_s values of the sampled coal ashes are shown in Fig. 2. The slagging behavior of Alaska coal and ROTO coal is quite high from the result of F_s value calculation of the candidate coal. For case of NOVA coal, an accurate fusion temperature can't be measured due to fusion temperature exceeds maximum temperature range of ash fusion determinator. But from the result of F_s value calculation, it is thought that NOVA ash sample doesn't show slagging characteristic in gasifier. Furthermore, result of R_s value calculation of the six coals doesn't represent any slagging behavior. But compared with the measurement of fusion temperature, F_s value and chemical composition data show slagging behavior in several coal samples. As a result, R_s values determined by Eqn. (2) and F_s values by Eqn. (3) illustrated somewhat different results of slagging behavior of coal ash.

Up to the present, coal ashes are manufactured by ASTM method and the slagging behavior of the coal ash is predicted by measuring its chemical composition and fusion temperature. But it is expected that the slag produced in actual gasifier is quite different from that by ASTM method. Because of complex processes in gasifier such as, higher heating rate and the volatilization of low melting ash component, precise prediction of slagging should be determined by measuring chemical composition, particle size, deposition rate of the slag produced by DTF, which represents simulated condition of an actual gasifier's temperature, gas composition and heating rate. With this finding in mind, a specially designed DTF is constructed to

determine actual slagging behavior of coal ash. It can get a heating rate of 10⁴K/sec and maximum temperature of 1900K close to real furnace. The schematic diagram of the DTF system is shown in Fig. 3. Steam generator was added to simulate gasifier condition. Deposit probe is also installed to get slag from main reactor tube. In the DTF, the ash transformation process of original coal is determined by analyzing ash produced with different residence time in DTF experiment. Distribution of inorganic materials in coal and thermal, chemical, physical characteristics of ash is also considered by analyzing molten ash produced by DTF. With deposition probe at the low part of DTF, deposition rate of molten slag is measured and composition, structure and strength of deposited ash on the probe is analyzed. All of the experimental data will be used to establish the ash slagging mechanism in coal gasifier condition.

CONCLUSION

Chemical compositions and ash fusion temperatures were determined for different coals which is presently used in Korean power plant. Relationship between measured value and slagging behavior was evaluated by calculating two different slagging parameters, Rs and Fs. Slagging indicator (Rs) and Fs (slagging index) evaluation result show somewhat contradictory behavior of ash slagging behavior due to standard ASTM ashing method doesn't represent actual gasifier slagging condition. As a result, precise slagging prediction of coal ash should be done with simulating gasifier condition such as one in DTF.

REFERENCE

1. *The Research of Combustion Characteristics in Domestic Thermal Power Plant*, Korea Institute of Energy Research, Report, 1993.
2. Clarence Karr, *Analytical Method for Coal and Coal Products*, Academic Press, 1978.
3. J. G. Singer, *Combustion Fossil Power Systems*, Combustion Engineering Inc., 1981.
4. Gray, R.J. and Moore, G.F, *Burning the sub-bituminous coals of Montana and Wyoming in large utility boilers*, ASME paper 74-WA/FV-1, 1974.

Table 1. Proximate & Ultimate Analysis of coal Ash samples

Coal	Proximate Analysis				Ultimate Analysis				
	M.	V.M.	F.C	Ash	C	H	O	N	S
ULAN	2.4	30.6	51.3	15.8	81.1	5.0	10.8	1.78	0.86
Palmo	2.6	18.7	63.8	15.4	86.3	4.3	8.2	0.47	0.32
NOVA	2.4	26.6	55.9	15.1	82.8	3.9	9.7	1.88	0.71
C&A	2.4	31.7	51.7	14.0	80.0	5.0	12.6	1.74	0.62
Alaska	16.67	35.1	35.1	8.7	60.5	5.9	30.8	2.19	0.24
ROTO	5.61	46.71	51.76	1.5	69.3	4.7	24.4	1.32	0.27

Table 2. Chemical Composition of coal Ash samples

#	Coal	SiO ₂	Al ₂ O ₃	TiO ₂	P ₂ O ₅	Fe ₂ O ₃	CaO	MgO	Na ₂ O	K ₂ O
1	ULAN	74.2	15.78	0.8	0.13	3.45	1.69	0.5	0.28	0.66
2	Palmo	66.9	20.52	0.92	0.26	4.56	1.49	0.51	0.25	0.72
3	Alaska	49.23	18.13	0.82	0.35	6.08	12.17	2.28	0.47	1.32
4	NOVA	62.53	28.64	1.21	0.29	1.19	0.25	0.26	0.07	1.88
5	C&A	57.75	23.00	1.02	0.44	4.1	2.23	0.94	0.41	1.52
6	ROTO	32.58	27.49	0.25	0.24	21.23	4.11	1.85	0.24	0.87

Table 3. Ash Fusion Temperature of coal Ash samples

	ULAN		Palmo		Alaska		NOVA		C&A		ROTO	
	Ox	Re	Ox	Re	Ox	Re	Ox	Re	Ox	Re	Ox	Re
IDT	1423	1423	1446	1414	1199	1154	>1600	>1600	1452	1373	1395	1204
ST	1478	1457	1494	1478	1222	1197	>1600	>1600	1489	1474	1424	1236
HT	1517	1476	1520	1499	1249	1217	>1600	>1600	1520	1498	1430	1257
FT	1566	1502	1538	1516	1283	1243	>1600	>1600	1541	1523	1437	1271

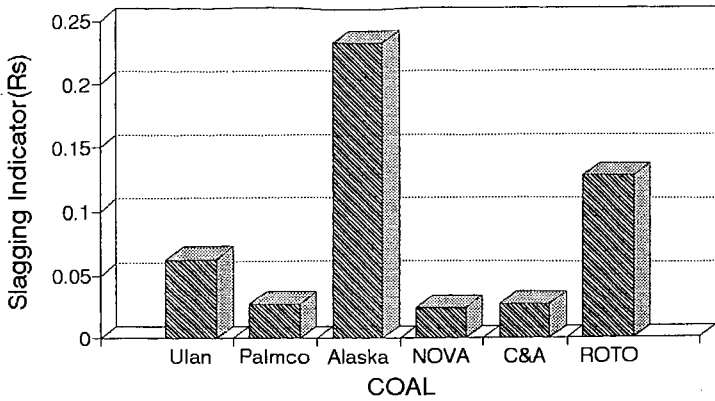


Fig. 1. Slagging Indicator (Rs) values of Six Different Coal Samples

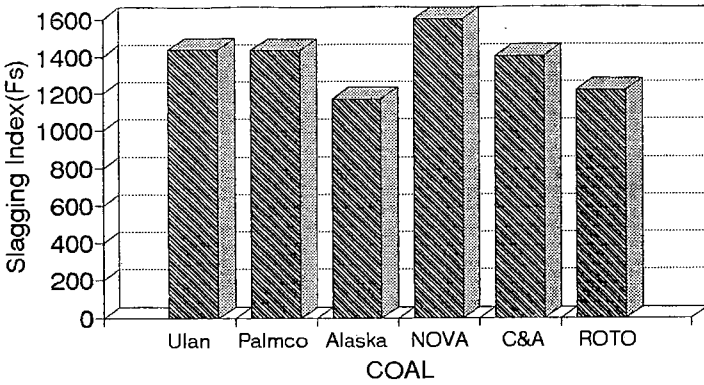


Fig. 2. Slagging Index (Fs) values of Six Different Coal Samples

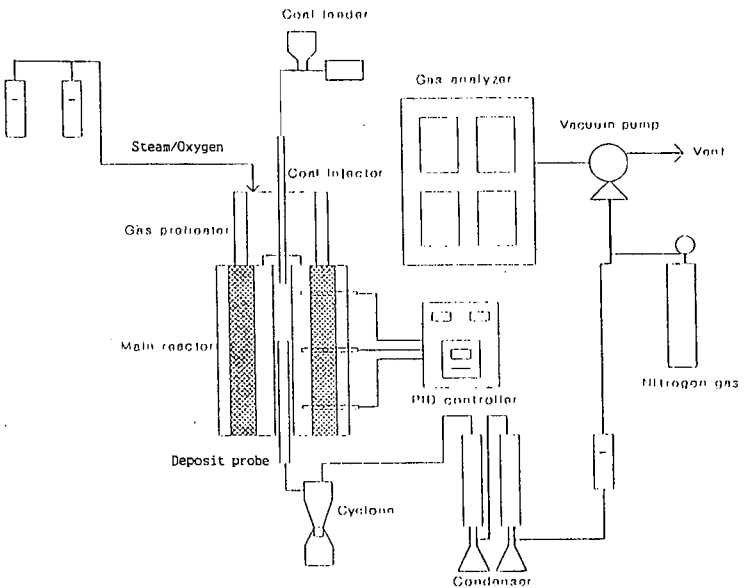


Fig. 3. Schematic Diagram of DTF

ION EXCHANGE AND ABSORPTION TECHNIQUES TO APPLY CATALYSTS FOR LIQUEFACTION OF LOWER RANK COALS

by Karl S. Vorres*, Donald C. Cronauer**, Christine W. Curtis***,
and Charles J. Brannan***

* CHM/211, Argonne National Laboratory, Argonne, IL 60439

** Amoco Research Center, P O Box 3011, Naperville, IL 60566

*** Department of Chemical Engineering, Auburn University, AL
36849-5127

ABSTRACT

Samples of Beulah-zap lignite, Black Thunder and Wyodak sub-bituminous, and Illinois #6 high volatile bituminous coals have been prepared by acid treatment to remove exchangeable cations. Subsequent treatments were made with solutions of catalytic metals including iron or cobalt or nickel to exchange with the acid sites, or with molybdate to adsorb on the surface. Samples were then subjected to liquefaction conditions in microautoclave tubular microreactors and solvent extraction was used to establish total conversion or yields of oils, asphaltenes and preasphaltenes. Results of the liquefaction experiments are compared with the catalyst loadings.

INTRODUCTION

The use of catalysts to improve the liquefaction of lower rank coals has a number of advantages. The disadvantages of cost and recovery of these metals has led to a study of methods of application which can place small amounts of metal on the coal to minimize the cost and need for recovery. A variety of techniques have been used for catalyst application, including blending, "incipient wetness", ion exchange and surface adsorption. This paper provides details of some recent work with the ion exchange and surface adsorption techniques and subsequent liquefaction experiments.

An earlier paper (1) has indicated the value of these techniques, and some structural aspects of ion exchange studies as part of the preparation for catalyst loading.

The coal structure of low rank coals is known to contain reactive functional group types including carboxylate and phenolic. The proportion of these groups decreases with increasing rank. The carboxylates are known to be able to act as ion-exchange materials. The functional groups are frequently linked to a variety of alkali and alkaline earth cations. The inorganic cations can be detrimental due to fouling of boilers during operation or reducing yields for liquefaction.

The latter deleterious effects of calcium in the coal (and any other exchangeable cations) can be overcome by removal of these species. A number of studies have indicated that low rank coals can be treated with acids to exchange the cation species with hydrogen ions (2-4). The cations can then be washed away from the coal to minimize their effect. A sulfurous acid treatment will also remove cations and prepare the the samples for ion exchange (5).

EXPERIMENTAL

Ion Exchange - Acid Washing

The samples were a Black Thunder mine (Wyoming) subbituminous coal and the Argonne Premium Beulah-Zap lignite, Wyodak sub-bituminous, Illinois #6 high volatile bituminous coals (6).

The acid washing treatments involved the three Argonne coal samples. The -20 mesh samples were dry screened to -20+200 mesh. Weighed amounts (about 30 grams) of the screened samples were slurried with deionized water. Fines (still -200 mesh) were decanted away from the slurry using about 200-600 ml of water. The slurry, containing about 15-20 grams of coal, was washed into a special 50 ml burette. The burette had been fitted with a coarse fritted glass disk at the 50 ml mark to retain the coal

but allow solutions to pass. Fine coal particles had to be removed to avoid pluggage of the frit. A siphon flow provided a uniform flow of 0.1 N HNO₃ (or H₂SO₄ for some of the Wyodak coal) to the sample. Acid flow rates were typically about 1-3 ml/minute and were set according to the ability of the solution to pass through the coal bed. Following the treatment with the acid, the samples were washed with distilled water fed by the siphon, and the record of pH and ion concentration was obtained in a manner similar to that for the acid treatment. The burette tip was fitted with tubing to connect a flow-through pH electrode from Cole-Parmer, or from Microelectrodes, Inc (Londonderry, NH) and with ion-selective electrodes for Ca⁺², Na⁺ and K⁺. The electrodes were used with an Orion EA940 pH meter. The pH meter in turn was connected to an IBM model AT computer for data acquisition. A program was written which allowed data points to be acquired at specific intervals in the range of 10-18 seconds. The data files were then manipulated with a word processor and Lotus 123 macros to permit plots to be drawn of the data.

For the Beulah-Zap and Illinois #6 coals, the calcite reacted with the acid to produce bubbles of carbon dioxide in the column. These bubbles tended to block the flow of acid. Therefore, an initial acid treatment was given before the burette studies for further samples. The acid wash was followed by a water rinse. Three cycles of acid wash and water rinse were used before the catalysts were added to the coals.

The Black Thunder sample was prepared by blending a large sample and screening to obtain a -8+20 fraction. This material was allowed to contact sulfurous acid for 4 hours. The acid and dissolved mineral matter were filtered and flushed with water. Samples of this treated coal were used for the catalyst loading.

Catalyst Loading

Catalyst materials were added by ion exchange or adsorption techniques. For the addition of Fe, Co or Ni, solutions containing 1000 ppm of metal were made up and added to acid washed coal samples. The solution of ferrous sulfate was acidified slightly to avoid precipitation of hydroxide species. The amount of solution used was twice the desired amount to be added for any of Fe, Co or Ni. This amount was added to the coal slurry, stirred well and allowed to exchange for up to about 42 hours. For the addition of Mo, the procedure developed by Schroeder was used (8). The Mo concentration used was 1500 ppm at a pH of 2. The adsorption is relatively rapid and provided the loadings indicated in Schroeder's procedure. Following reaction with the coal the catalyst solution was washed from the coal with several volumes of distilled or deionized water. The weighed solution was then analyzed for concentrations of the catalyst materials. Catalyst loadings were determined from the difference in the amount of material in the initial and final solutions.

Liquefaction Studies

Initial coal samples (comparing raw, water washed and acid washed) were liquefied in tubular microreactors to establish yields based on THF solubility (total conversion) and heptane solubility (oil yield). Conditions were: solvent 1-Methyl Naphthalene (non-donor), 2:1 solvent:coal; 425 C, 30 minute reaction, cold charge at 1000 psi H₂, (1700-1800 hot), reactor volume of about 20 cm³. The reactor charge was 2g of 1-methylnaphthalene as the reaction solvent and 1.33 g maf coal. Later tests with catalyst-loaded samples included 0.67 g pyrene as a test hydrogenation compound.

For the Wyodak samples, some runs were made with a process-derived solvent, designated V1074, obtained from the Wilsonville, Alabama liquefaction pilot plant. A hydrogen donor solvent, dihydroanthracene (DHA), was also used for comparison.

The products from the liquefaction reactions were removed from the reactor with THF. Conversion of coal to THF solubles was determined. In the initial test the residue solubility in heptane was also determined. For the catalyst-loaded samples the amount of pyrene hydrogenation to hydrogenated products that occurred in the reactions was obtained by gas chromatographic

analyses using a Varian Model 3400 equipped with a J&W DB-5 fused silica 30-m column and flame ionization detection.

RESULTS AND DISCUSSION

Ion Exchange

The readings from the electrodes indicated that the coals were washed free of exchangeable cations with the exception of calcium after the first cycle. The calcium came out during the water rinse over a pH range of 1.5-2.5. The possibility of calcium in the clay of the samples is assumed from this data. Additional calcium was removed during the later cycles using either the acid or the rinse water. The final concentrations were micromolar.

Liquefaction Studies

Initial runs were made to compare fresh material from ampules and acid treated Wyodak samples. Samples of the raw coal were compared with both water-washed and acid-washed Wyodak samples. Ash values were also obtained. The water-washed and acid washed samples were dried before the ash determination. The results are summarized below.

Values in %				
Coal Sample	moisture	ash	dry ash	reduction
Raw	27.39	6.31	8.69	0
Water washed	6.4	7.81	8.34	4.0
Acid washed	6.96	3.46	3.72	57.2

These microreactor liquefaction results are summarized below.

Raw Sample	THF soluble (total conv.)	Heptane soluble (oil yield)
Raw	55.2, 56.1	34
Water Washed	44	27
Acid washed	37	24

The total conversion and oil yields of the three initial samples decreased with the extent of treatment. This effect may be due to the amount of handling, which increases oxidation. The samples were kept under a layer of water to avoid oxidation.

Samples of acid washed Beulah-Zap, Wyodak and Illinois #6 were compared in several solvents.

The results for total conversion are indicated below:

Coal	1 MeNap.	V1074	DHA
Beulah-Zap	73.5	74.1	86.7
Wyodak	71.4	85.9	86.9
Illinois #6	86.4	86.5	86.4

The reaction conditions were: 410°C, 30 min., no catalyst and 1250 psig H₂ introduced at ambient temperature.

The Illinois #6 sample gave consistent relatively high total conversions. This sample had the highest total sulfur content in these coals. For the Wyodak coal the process derived solvent and the hydrogen donor solvent gave very similar total conversions, while the non-hydrogen donor solvent gave lower conversions. For the Beulah-Zap coal, the non-donor solvent and process-derived solvent gave very similar conversions which were less than that obtained with the hydrogen donor solvent, dihydroanthracene (DHA). The DHA gave very similar total conversions with each of the coals. The maf organic sulfur % values for the Illinois #6, Wyodak and Beulah-Zap are: 2.38, 0.47 and 0.70. The pyritic sulfur values are: 2.81, 0.17 and 0.14.

Subsequent catalyst loading produced a series of samples in several batches to give a variety of loadings in the 100-1000 ppm range. These were also run in microautoclave tubing reactors to establish liquefaction yields based on THF solubility (total conversion) and pyrene conversion (catalyst reactivity).

The samples prepared with Ni and Co were run about one month after preparation, and the others about two months after.

The results of duplicate runs are given below:

Sample	1st Cat. Ldg.	2nd Cat. Ldg.	Ave. Coal Conv.	Ave. Pyrene Conv.
--------	---------------------	---------------------	-----------------------	-------------------------

Black Thunder

One catalyst metal

BT-1-Mo	829		65.5	5.3
BT-1-Fe	548		60.1	3.4
BT-1-Co	212		63.3	2.9
BT-1-Ni	257		64.0	2.6

BT-2-Mo	418		63.3	3.1
BT-2-Fe	483		65.9	3.0
BT-2-Co	83		65.1	2.9
BT-2-Ni	464		66.0	2.9

Two catalyst metals

Fe-Mo-1	456	210	69.1	5.3
Fe-Mo-2	484	70	66.5	4.8
Fe-Ni-1	408	224	67.5	3.9
Fe-Ni-2	472	106	66.4	4.0

Wyodak Samples

Wyodak, raw (no washing)	none		71.4	2.0
-----------------------------	------	--	------	-----

Wyodak, (nitric acid washed)	none		41.6	3.1
---------------------------------	------	--	------	-----

(Sulfuric acid washed)

WY-Mo	847		74.2	4.5
WY-Fe	552		74.7	3.3
WY-Co	668		53.3	2.5
WY-Ni	822		75.5	3.1

Cobalt was much more difficult to get on the coal than the Fe or Ni. The analyses of metal loadings are good to 10%. Individual determination values ranged up to 4% different from the averages.

For the Black Thunder coal, regardless of the metal type, metal loading or batch, the coal conversion was very similar and ranged for individual determinations from a low of 59% for Fe batch 1 to a high of 70% for Ni batch 2. The coal conversions for the combined metals were slightly higher and less variable than the individual metals. Pyrene conversions tended to be higher for the combined metals than for individual ones.

Wyodak coal which had been acid washed with H_2SO_4 , with the exception of the Co treated sample, gave higher coal conversions than the Black Thunder samples. The primary hydrogenation product produced in each reaction was dihydropyrene. The overall conversions do not appear to be as high as reported for a number of other catalyst preparations. The comparison sample of Wyodak which had been acid washed, but with nitric acid, gave substantially lower total conversion. This may reflect the state of oxidation of the coal.

The pyrene conversion, an indicator of hydrogenation activity, was highest for the Mo catalyst preparations.

CONCLUSIONS:

1. Catalytic metals including Fe, Ni and Co as well as Mo can be placed on lower rank coals following an acid wash in a wide range of concentrations.
2. Comparisons of raw, water washed and acid washed sub-bituminous samples show reduced yields for more significant treatment.

3. The preparations with different catalysts tended to give similar total conversions.
4. Somewhat higher conversions for the Wyodak coal were obtained from samples which had been treated with sulfuric acid to remove exchangeable cations.
5. Conversions were uniformly high with all solvents for the highest rank samples. Lower rank conversions were lower for the non-donor solvent and also, for the lignite, for the process derived solvent.

ACKNOWLEDGMENTS

KSV acknowledges with thanks the support from the U S Department of Energy, Office of Fossil Energy, and data as well as discussions with Anthony Cugini of the US DOE Pittsburgh Energy and Technology Center.

REFERENCES

1. K. S. Vorres, Prepr. Fuel Chem. Div., ACS, 1993, 38 (3) 1045-1051
2. C. Lafferty and M. Hobday, Fuel, 69, 78-83 (1990)
3. C. Lafferty and M. Hobday, Fuel, 69, 84-87 (1990)
4. J. T. Joseph and T. R. Forrai, Fuel, 71, 75-80 (1992)
5. C. J. Brannan and C. W. Curtis, Prepr. Fuel Chem. Div., ACS, 1993, 38 (3) 1001-1007
6. K. S. Vorres, Energy Fuels, 4, 420-426 (1990).
7. K. S. Vorres, Users Handbook for the Argonne Premium Coal Sample Program, 1993, 27, taken from R. D. Harvey, Ill. State Geol. Survey, 1988.
8. K. Schroeder, Prepr. Fuel Chem. Div., ACS 1993, (2) 512